Journal of Medicinal Chemistry

Article

Discovery of LX2761, a Sodium-dependent Glucose Cotransporter 1 (SGLT1) Inhibitor Restricted to the Intestinal Lumen, for the Treatment of Diabetes.

Nicole C Goodwin, Zhi-Ming Ding, Bryce A Harrison, Eric D. Strobel, Angela L. Harris, Melinda Smith, Andrea Y. Thompson, Wendy Xiong, Faika Mseeh, Debra J Bruce, Damaris Diaz, Suma Gopinathan, Ling Li, Emily O'Neill, Mary Thiel, Alan G.E. Wilson, Kenneth G Carson, David R. Powell, and David B Rawlins

J. Med. Chem., **Just Accepted Manuscript** • Publication Date (Web): 03 Jan 2017

ACS Publications

Journal of Medicinal Chemistry is published by the American Chemical Society. 1155 Sixteenth Street N.W., Washington, DC 20036

Discovery of LX2761, a Sodium-dependent Glucose Cotransporter 1 (SGLT1) Inhibitor Restricted to the Intestinal Lumen, for the Treatment of Diabetes.

Nicole C. Goodwin,[*,†] Zhi-Ming Ding,[‡] Bryce A. Harrison,[†] Eric D. Strobel,[†] Angela L. Harris,[‡] Melinda Smith,[‡] Andrea Y. Thompson,[‡] Wendy Xiong,[‡] Faika Mseeh,[§] Debra J. Bruce,[ǀ] Damaris Diaz,[ǀ] Suma Gopinathan,[ǀ] Ling Li,[ǀ] Emily O'Neill,[ǀ] Mary Thiel,[ǀ] Alan G. E. Wilson,[ǀ] Kenneth G. Carson,[†] David R. Powell,[‡] David B. Rawlins,[†]

[†] Department of Medicinal Chemistry, Lexicon Pharmaceuticals, 110 Allen Road, Basking Ridge, New Jersey, 07920.

[‡] Department of Metabolism Research, [§] Department of Pharmaceutical Discovery, and [ǀ] Department of Drug Metabolism, Pharmacokinetics, and Toxicology, Lexicon Pharmaceuticals, 8800 Technology Forest Place, The Woodlands, Texas, 77381.

RECEIVED DATE (will be automatically inserted after manuscript is accepted).

Abstract. The increasing number of people afflicted with diabetes throughout the world is a major health issue. Inhibitors of the sodium-dependent glucose cotransporters (SGLT) have appeared as viable therapeutics to control blood glucose levels in diabetic patents. Herein we report the discovery of LX2761, a locally-acting SGLT1 inhibitor that is highly potent in vitro and delays intestinal glucose absorption in vivo to improve glycemic control.

Introduction. The prevalence of diabetes has become an increasing concern to the world's population. In 2012, the World Health Organization reported that the incidence of the disease was estimated to be 9% in adults over the age of 18. That number is expected to rise due to population growth, an aging population, and lifestyle tendencies that have led to an increase in obesity. Diabetes is projected to be the seventh leading cause of death by 2030.[1] It is a metabolic syndrome characterized by hyperglycemia, which results either from an absolute deficiency in insulin secretion (type 1 diabetes) or

from resistance to insulin action combined with an inadequate compensatory increase in insulin secretion (type 2 diabetes). Chronic hyperglycemia is a major risk factor for microvascular complications resulting in retinopathy, nephropathy, and neuropathy, and contributes to macrovascular complications leading to cardiovascular disease.[2] Current therapies aimed at aggressive glycemic control are often accompanied with side effects, most notably weight gain and severe hypoglycemia, which may, in turn, be associated with an increased incidence of cardiovascular events. Additional treatments to aid in glycemic control are essential to prevent the associated mortality and morbidity of this disease.[3,4]

The potential of sodium-dependent glucose cotransporters (SGLTs) as a new family of drug targets for the treatment of diabetes has been realized over the past few decades.[5,6] The SGLT family consists of several isoforms that actively transport sugars across cellular membranes, a process that is coupled with sodium ion transport.[7,8] SGLT1 is primarily expressed in the gastrointestinal (GI) tract where it is largely responsible for intestinal absorption of glucose and galactose.[9,10] SGLT1 is also present in the proximal straight tubule of the kidney where it helps to absorbs plasma glucose filtered from the blood. In contrast, SGLT2 is primarily expressed upstream of SGLT1 in the proximal convoluted tubule of the kidney.[11] Under normal physiologic conditions, greater than 97-98% of the plasma glucose filtered in the kidney is reabsorbed, and SGLT2 is responsible for approximately 90% of this reabsorption. Any glucose not reabsorbed by SGLT2 is reabsorbed by SGLT1 or excreted into the urine. Humans with inactivating SGLT2 mutations present with significant glucosuria but are otherwise healthy.[12,13] Humans[14] and mice[15] with inactivating SGLT1 mutations have minimal increase in glucosuria but exhibit glucose-galactose malabsorption (GGM),[16] a serious GI condition characterized by diarrhea induced by the inability to absorb these sugars from the gut. The GGM phenotype can be mitigated through early detection and dietary modifications, and individuals lacking SGLT1 appear to gradually tolerate the introduction of glucose into their diet as they age.[17] No other phenotypes are noted in individuals with an SGLT1 genetic deficiency.

The focus of industrial programs has been on selective SGLT2 inhibition and several glucose-based small molecules have been approved by the FDA for the treatment of diabetes.[5,18,19]

Dapagliflozin[20-22] and canagliflozin[23-26] were both approved by the FDA in 2013 and empagliflozin[27,28] was approved in 2014. In addition, ipragliflozin,[29-31] luseogliflozin,[32-34] and tofogliflozin[35-37] have all been approved in Japan. (Fig. 1).

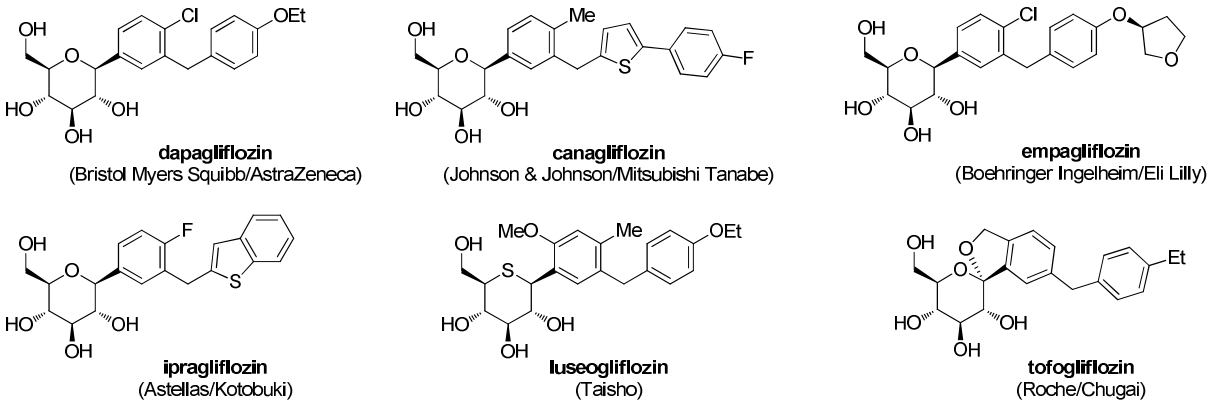

Figure 1. Marketed SGLT2 inhibitors (2016).

Using our proprietary mouse knockout (KO) technology,[38,39] we independently confirmed that both SGLT1 and SGLT2 KO mice have strong anti-diabetic phenotypes.[40] Analogous to humans, mice lacking SGLT2 had improved glycemic control due to an increase in urinary glucose excretion (UGE). SGLT1 KO mice, when challenged with a glucose-containing meal, displayed decreased postprandial glucose (PPG) excursions, increased cecal glucose, and increased circulating glucagon-like peptide-1 (GLP-1) levels, all consistent with delayed glucose absorption.[41] Decreased PPG will improve glycemic control, and, in addition, increased circulating GLP-1 may further improve glycemic control through the same mechanisms activated by GLP-1 analogs and by the increased GLP-1 levels that result from treatment with dipeptidyl peptidase 4 (DPP4) inhibitors such as sitagliptin.[42] The added benefit of inhibiting the SGLT1 pathway compelled us to develop sotagliflozin, also known as LX4211 (**1**, Fig. 2), a dual SGLT1 and SGLT2 inhibitor currently in late-stage clinical development for diabetes.[43] Sotagliflozin treatment significantly improves glycemic control in patients with diabetes, and this improvement has been accompanied by a very favorable safety profile. Of particular note, diabetic

patients treated with compound **1** have not exhibited an increased frequency of diarrhea, a side effect that might be expected from SGLT1 inhibition.[44-48]

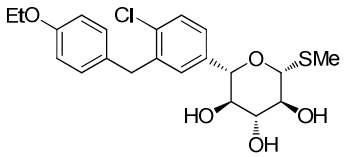

Figure 2. Sotagliflozin (**1**), a dual SGLT1/2 inhibitor in clinical trials for type 1 and type 2 diabetes.

The potential of enhanced glycemic control through SGLT1 inhibition was attractive because it would provide an alternative approach to glycemic control that was not dependent on kidney function. Current SGLT2 selective inhibitors lose efficacy in patients with moderate to severe renal impairment, which affects 30-40% of all diabetic patients.[49-51] Although compound **1** at maximal clinical dose works through this pathway by partially inhibiting intestinal SGLT1,[48] a more potent SGLT1 inhibitor that is restricted to the intestine could potentially be titrated to a dose that provides even greater glycemic control through this mechanism before GI side effects occur, and would also avoid the glycosuria-related side effects of SGLT2 inhibitors, particularly genital tract infections.

Design of an SGLT1 inhibitor began with the thiomethyl xyloside core of **1** because that particular anomeric substitution imparted a unique potency at SGLT1 where other xylose and glucose cores did not.[52] To our knowledge at the time, no compound selective for SGLT1 over SGLT2 in vitro had been reported.[53] Therefore, we focused our strategy on obtaining an SGLT1 selectivity profile based on its in vivo expression where SGLT1, but not SGLT2, is expressed in the GI tract. We set out to design a compound that would remain within the GI tract due to poor oral bioavailability. When we commenced our chemistry effort sing this strategy, there were a few reported examples in the patent literature that described the development of dual SGLT1 and SGLT2 inhibitors that targeted both SGLT1 in the intestinal tract and both SGLT1 and SGLT2 in the kidney.[54-56] Since then, Kissei has reported their similar strategy for *O*-glycosides that are SGLT1 inhibitors.[57-59]

Compounds of interest were required to demonstrate certain characteristics that are briefly introduced here and will be discussed in detail in the following section. First, the compounds must display high in vitro potency at SGLT1 in cellular assays. Second, these potent inhibitors must have efficacy in vivo, specifically in a mouse oral glucose challenge where the critical endpoints were decreased glucose excursion accompanied by increased cecal glucose and total plasma GLP-1 (tGLP-1) levels, all of which indicate delayed intestinal glucose absorption from SGLT1 inhibition. Finally, the compounds must display low systemic exposure determined directly through pharmacokinetic assessment and indirectly through measurement of low UGE. As all of our compounds were potent inhibitors of SGLT2 in addition to SGLT1, any significant absorption into the systemic circulation would increase UGE by inhibiting SGLT1 and SGLT2 in the kidneys, thus negating the in vivo selectivity that we desired by sequestration of the compound to the GI tract.

SAR and In Vitro Activity. In our efforts to find non-absorbable inhibitors of SGLT1, we chose to keep the xyloside core of **1** intact while altering physical properties by doing structure-activity relationships (SAR) on the bisaryl aglycon moiety. As highlighted in Figure 3, chemical exploration was conducted at three different positions: (1) the substitution "X" at the proximal aryl ring, (2) linker "Y" of the distal aromatic ring with varying tether lengths "n", and (3) distal functionality "Z" at the end of the tether which would be used to modulate the physical properties.

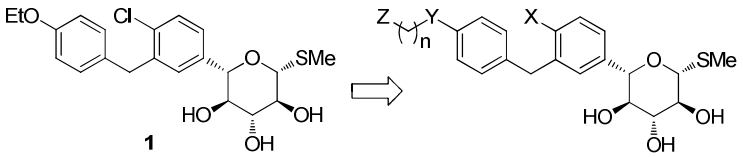

Figure 3. Synthetic strategy to design a compound that is restricted to the lumen starting with the xyloside core of **1**.

Surprisingly and gratifyingly, modifications at these positions provided quick access to compounds that were extremely potent at human SGLT1 and SGLT2.[41] It is worth noting that tuning the selectivity to significantly favor SGLT1 inhibition over SGLT2 inhibition was never observed in this

program. Substitution on the proximal aryl ring (Fig. 3, "X") was explored as either X = Me or Cl. The methyl substitution at this position was ultimately preferred for its slightly higher potency at SGLT1 but, more importantly, for its compatibility with synthesis and starting material availability. The linker at the distal aromatic ring (Fig. 3, "Y") was explored with either Y = O or CH_2. Both of these substitutions were interchangeable in terms of their potency at SGLT1/2. The most influential position in establishing potency at hSGLT1 in this series was the functional group (Fig. 3, "Z") appended to the distal aromatic ring of the aglycon moiety. In addition to providing potency, installation of polar and charged functional groups were utilized to limit oral absorption of the compounds.[60]

Table 1. Representative SAR of non-absorbable dual SGLT1/2 inhibitors.

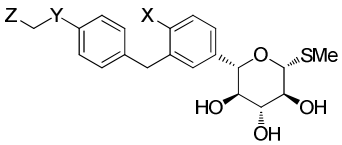

Cmpd	X	Y	Z	IC_{50} (nM) hSGLT1	IC_{50} (nM) hSGLT2	%F[a]
1	Cl	O	Me	36.2	1.8	98
2	Cl	O	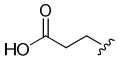	250	4.3	
3	Me	O	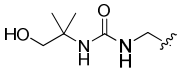	48.2	3.7	
4	Me	O	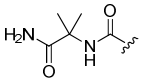	25.3	5.2	
5	Me	O		15.4	14.5	18
6	Cl	O	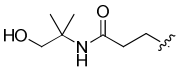	2.4	0.9	17
7	Me	O	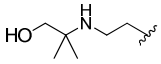	3.3	2.5	1.1
8	Me	O	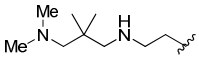	2.0	1.6	BLQ
9	Me	CH_2	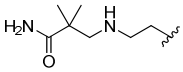	2.3	3.6	0.5
10	Me	O	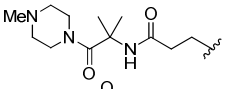	2.9	3.7	0.4
11	Me	CH_2	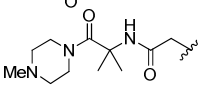	1.8	1.9	BLQ

[a] measured at 10mpk, PO. BLQ = not available due to insufficient compound level in plasma

A brief summary of substitution at the "Z" position is shown in Table 1. Simple carboxylic acids (**2**) were universally not tolerated at hSGLT1. Otherwise, a large variety of functionality was tolerated but needed to be positioned more than 2 linker atoms away from the aryl ring (**3** and **4**) to maintain potency. In addition, combinations of neutral groups were not enough to render these compounds restricted from systemic circulation (e.g. %F = 18% and 17% for diol **5** and amide **6**, respectively). Installation of basic amines that would have a net charge under physiochemical conditions was beneficial to decrease the

permeability of these compounds (amines **7** – **8**, %F = <2%) without sacrificing cellular potency. A series of compounds that featured amides and charged amines (**9** – **11**) were designed and proved to be extremely potent in vitro and exhibited oral bioavailabilities that were a fraction of a percent.

Further pharmacodynamic evaluation of these compounds revealed that, for reasons that are unclear, the bisamides with a basic amine, such as piperidine amides **10** and **11**, were more efficacious in vivo than amines **7** - **9**. In particular, piperidinylamide **11** was identified as an early lead compound and required scale-up of gram quantities for further in vivo profiling. However, upon scale-up of amide **11**, a synthetic instability of the bisamide motif was observed under acidic conditions in protic solvent. As shown in Figure 4, exposure of **11** to acidic methanolic solutions initiated a selective methanolysis of the terminal amide to methyl ester **13** and insignificant amounts of the other potential methanolysis product **14** were observed. This regioselective decomposition was hypothesized to be occurring via oxazolone intermediate **12** to favor formation of ester **13** in a selective decomposition pathway. In order to confirm this degradation pathway, ^{13}C NMR was used to detect the presence of the oxazolone intermediate **12**. Bisamide **11** was exposed to catalytic amounts of deuterium chloride (35 wt% in D_2O) in deuterated methanol, and the emergence of a new peak characteristic of an oxazolone (^{13}C δ = 165 ppm) was observed and then followed by conversion to the methyl ester **13** (^{13}C δ = 172 ppm). Although this hydrolysis was not observed during in vivo PK studies or in forced stability studies with simulated gastric fluid or simulated intestinal fluids at 50 °C, we felt the stability would complicate future synthetic chemistry development.

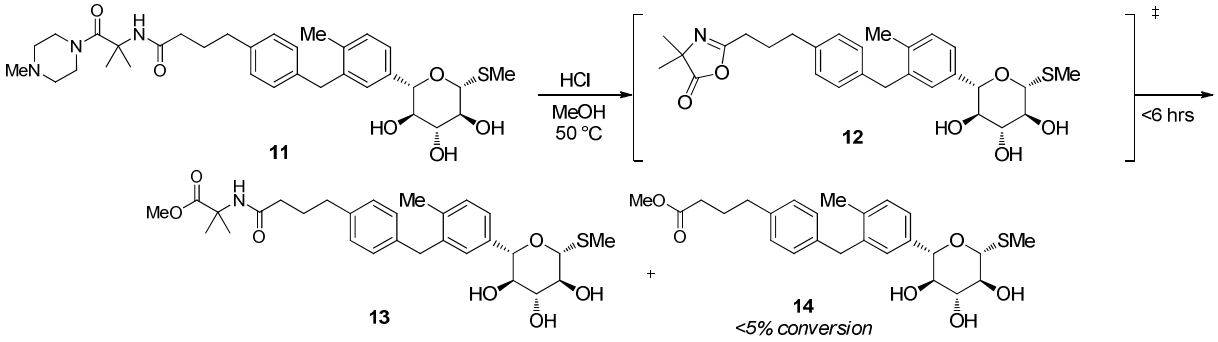

Figure 4. Synthetic instability of piperazinylamide **11**.

Consequently, compounds were synthesized that would disfavor or eliminate the formation of the oxazolone intermediate **12** in order to render these compounds synthetically stable. All compounds shown in Table 2 maintained low nanomolar in vitro potency against SGLT1 and were thus triaged by their stability in accelerated degradation conditions (0.5*N* HCl in 1:1 methanol/water at 50 °C for 72 hours). Compounds that exhibited less than 5% degradation were considered to have acceptable stability.

Table 2. Stability of replacements to the hydrolytically-labile bis-amide motif of **11**

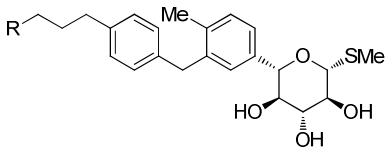

Cmpd	R	IC_{50} (nM) hSGLT1	IC_{50} (nM) hSGLT2	stable to hydrolysis?[a]
11	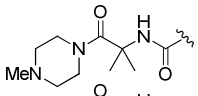	1.8	1.9	no[b]
15	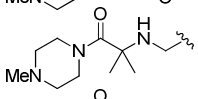	14.8	3.1	yes[c]
16	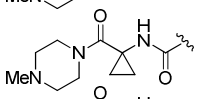	1.1	2.5	no
17	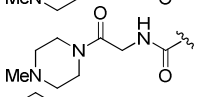	8.4	2.5	no
18	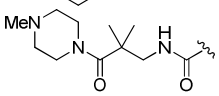	6.8	3.4	no
19	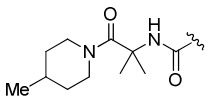	1.6	2.5	no
20	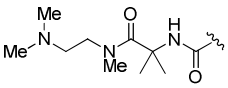	1.7	1.3	yes
21	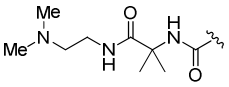	2.2	2.7	yes
22	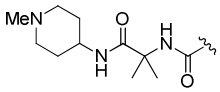	2.7	3.7	yes

[a] 50/50 1N aq. HCl/MeOH, 50 °C, 72 hrs. [b] >5% degradation. [c] <5% degradation

Compound **15** removed the carbonyl required to form the oxazolone ring of intermediate **12** and, as expected, **15** was stable to hydrolysis but lost in vitro activity at hSGLT1. Compounds **16-18** were designed to alleviate the Thorpe-Ingold effect, whereby geminal dimethyl substitution promotes intramolecular cyclization reactions.[61,62] In compound **16**, replacement of the dimethyl substitution of **11** with a cyclopropyl should increase the bond angle at the carbon and thus kinetically decrease the rate of oxazolone formation. In **17**, the dimethyl substitution was removed altogether, and in **18**, an extra

methylene was inserted in expectation that the six-membered oxazinone ring should have a relatively slower rate of formation than the corresponding five-membered oxazolone ring. All three of these compounds did indeed exhibit slower rates of acidic hydrolysis, however, none were sufficiently stable for the purposes of this program.

The last approach examined the electronic nature of the terminal carbonyl. As shown in Figure 5A, we hypothesized that acidic conditions could enforce a boat conformation through a bridging intramolecular hydrogen bond. The nitrogen lone pairs would no longer be in conjugation with the carbonyl and thus increase the electrophilicity of the amide and its susceptibility to nucleophilic attack. Piperidine amide **19** was expected to be stable because it cannot adopt the conformation shown in Figure 5A. To our surprise, it was just as unstable as piperazinylamide **11**, thus causing us to amend our hypothesis. A simple steric argument is shown in Figure 5B. The cyclic amide has an unfavorable interaction with the gem-dimethyl group if the nitrogen lone pair retains some sp^2-character in conjugation with the carbonyl. Rotation about the *N*-carbonyl bond would alleviate this steric interaction and remove the sp^2 character of the nitrogen, thus causing the carbonyl to be more reactive and susceptible to nucleophilic attack of the neighboring amide. Therefore, if the amide were to be either an uncyclized tertiary amide (**20**) or a secondary amide (**21** and **22**), it should be stable under acidic conditions. Gratifyingly, compounds **20** – **22** not only exhibited stability past 72 hours in our accelerated hydrolysis conditions, but they retained also excellent potency at both hSGLT1 and hSGLT2.

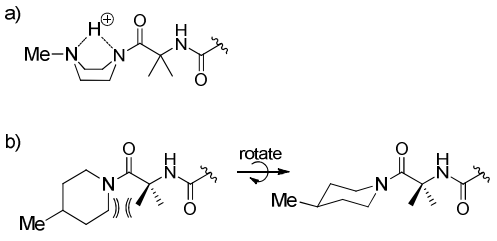

Figure 5. Destabilizing conformations of cyclic amides. (A) Acid-promoted conformational change of piperidinylamide engages nitrogen lone pair and destabilizes the carbonyl. (B) Unfavorable steric

interaction of piperidinyl-amide with gem-dimethyl group favors a conformation that removes the nitrogen lone pair from conjugation with the carbonyl.

The stable compounds from Table 2 were compared in a single dose oral glucose tolerance test (OGTT). Compound 21 ultimately emerged as a very potent, chemically-stable, and luminally-restricted molecule that achieved proof of concept in OGTT at very low doses. Based on the PK and PD data that is discussed in detail in the following section, *N*-(1-((2-(dimethylamino)ethyl)amino)-2-methyl-1-oxopropan-2-yl)-4-(4-(2-methyl-5-((2*S*,3*R*,4*R*,5*S*,6*R*)-3,4,5-trihydroxy-6-(methylthio)tetrahydro-2H-pyran-2-yl)benzyl)phenyl)butanamide (**21**) was nominated as preclinical candidate LX2761.[63]

Results and Discussion.

In order to assess the potency of these SGLT1 inhibitors in an oral glucose challenge, male C57 mice were fed a low-fat diet (10% lard fat, 35% sucrose) for six days prior to dosing the SGLT1 inhibitors by oral gavage once daily for four consecutive days. At 22 hours after the last dose of inhibitor and at 16 hours after food was removed, the mice were challenged with a glucose-containing meal administered by oral gavage. Blood samples were collected via retro-orbital bleeding at various time points within the first hour post-challenge and the test subjects were necropsied at the end of that hour. Necropsies provided measurement of cecal glucose and cecal pH levels while blood sampling provided blood glucose and plasma tGLP-1 levels.

The results from the oral glucose challenge are shown below in Figure 6. Mice treated with **21** exhibited a significant reduction in glucose excursion compared to vehicle and a significant increase in postprandial circulating levels of tGLP-1. As expected with a delayed glucose absorption that is mechanistic of SGLT1 inhibition in the intestine, mice treated with **21** exhibited a significant increase in cecal glucose levels and decrease in cecal pH due to fermentation of glucose to short chain fatty acids in the cecum. The magnitude of these effects recapitulates the magnitudes observed in our previously reported studies with SGLT1 KO mice.[41]

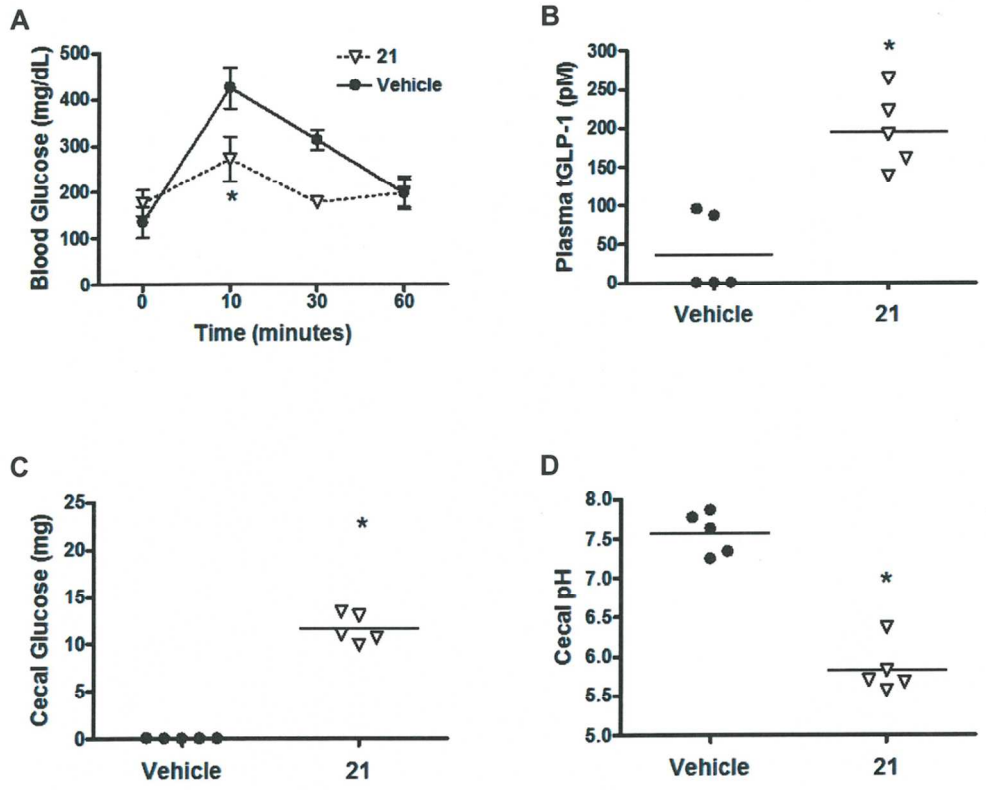

Figure 6. **Compound 21 delays intestinal glucose absorption and increases postprandial tGLP-1 levels in mice.** Individual healthy mice received either vehicle (●) or **21** at a dose of 1.5 mg/kg (**21,** △) by oral gavage for 4 consecutive days and then, 22 hours later after a 16 hour fast, received a glucose-containing meal challenge by oral gavage. A) Blood samples were collected through retro-orbital bleeding at 0, 10 30 and 60 minutes after meal challenge, and glucose AUC was calculated for each glucose excursion. At 60 minutes after the meal challenge (23 hours after the dose of compound or vehicle), mice were necropsied; blood samples collected at that time were used to measure B) plasma tGLP-1 levels, and cecal contents collected at that time were analyzed for C) total cecal glucose and D) cecal pH. * Different from vehicle, $P < 0.001$.

Compound **21** was designed to remain in the intestine after oral delivery to inhibit SGLT1 locally without affecting the SGLT1/2 mechanism in the kidney. The results of mouse pharmacokinetic (PK) studies are summarized below in Figure 7 using the structurally similar and orally bioavailable compound

1 as an internal reference. After oral administration at 10 mg/kg, **21** exhibited limited bioavailability with negligible concentrations detected in the plasma. Figure 8 shows the striking difference of plasma compound levels over time after oral dosing of compounds **21** and **1**, which in contrast affected high exposure and bioavailability in mice (C_{max} of 43 and 4073 nM, %F of <2 and 98%, respectively). Even upon escalating the oral dose of **21**, plasma exposure of the compound still remained very low.

	dose	*N*	half life	$AUC_{0-\infty}$	V_{ss}	CL
I.V.	*mg/kg*		*hr*	*nM*hr*	*L/kg*	*mL/min/kg*
compound **21**	1	4	0.4 ± 0.0	693 ± 107	1.3 ± 0.3	40.3 ± 6.6
compound **1**	1	4	1.39 ± 0.45	1940 ± 331	2.07 ± 0.14	20.6 ± 3.0

CL, clearance; *N*, number of animals, V_{ss}, volume at steady state

	dose	*N*	half life	C_{max}	$AUC_{0-\infty}$	%F
P.O.	*mg/kg*		*hr*	*nM*	*nM*hr*	
compound **21**	10	4	N/A	43 ± 11	N/A	N/A
compound **1**	10	4	6.52 ± 0.82	4973 ± 408	19709 ± 1580	98 ± 8

N/A, not available due to lack of terminal phase or insufficient compound levels in plasma

Figure 7. Pharmacokinetic data comparing compounds **21** and **1** at 1mg/kg IV and 10 mg/kg (PO).

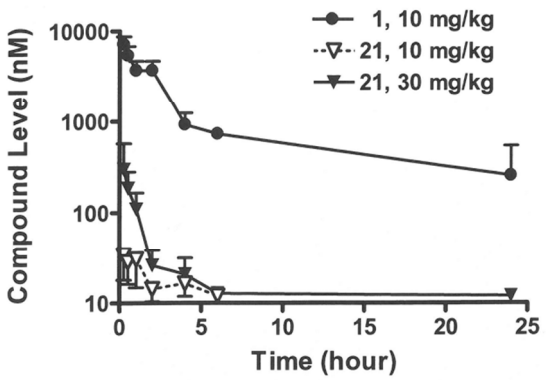

Figure 8. Plasma concentration-time course comparing compounds **21** and **1** at 10 and 30 mg/kg after oral administration.

Lastly, in order to further support the hypothesis that **21** was restricted to the intestines and not absorbed into the systemic circulation, this compound was compared to **1** for its ability to increase UGE in mice. If **21** was present in the systemic circulation, it would be expected to increase UGE due to its

potent inhibitory activity at both SGLT1 and SGLT2 in the kidneys[64] As shown in Figure 9, **21** had little effect on UGE when measured for 2 days after mice received a single 1.5 mg/kg dose (day 0) of **21** by oral gavage. As with the PK discussed previously, it is striking to compare this to **1** at the same dose. During the 24 hours after compound dosing, **1** increased UGE by 453 ± 77 mg/day while 2**1** increased UGE by a trivial 4 ± 9 mg/day.

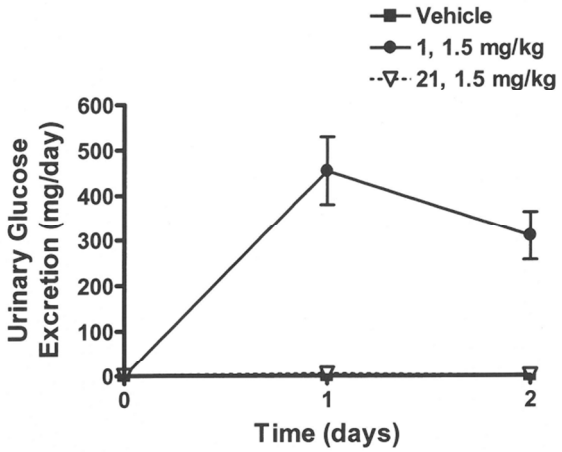

Figure 9. Urinary glucose excretion comparing a single 1.5 mg/kg dose of **21** and **1** before (day 0) and after (days 1 and 2) administration by oral gavage.

Chemistry. The medicinal chemistry synthesis of xyloside bisamide **21** is shown in Scheme 1. Synthesis of aryl chloride aglycon **26** began with the formation of Weinreb amide **24** of 2-methyl-5-bromobenzoic acid **23** through an acid chloride intermediate. Addition of *p*-chlorophenylmagnesium chloride into Weinreb amide **24** provided the corresponding bisaryl ketone **25**, which was then reduced using triethylsilane in the presence of $BF_3.OEt_2$ to furnish the aglycon **26**. Lithium/bromide exchange of **26** at −78 ºC with *n*-butyllithium generated the aryl lithium species which was subsequently added to the magnesium salt of morpholinoamide **27**[65] to cleanly yield ketone **28**. A diastereoselective reduction of the ketone under Luche conditions gave alcohol **29** in >20:1 ratio for the newly created diastereomeric center. Refluxing alcohol **29** in aqueous acetic acid resulted in a concomitant acetonide deprotection and

rearrangement to the pyran, which was then peracetylated to provide the crystalline tetracetate **30**. Diastereoselective installation of the thiomethyl beta-anomer of thioxyloside **31** was accomplished in a two-step, one-pot procedure. The anomeric acetate mixture of **30** was subjected to TMSOTf to generate the transient oxocarbenium ion. The neighboring acetate at the 2-position blocks the α face of the sugar, allowing for a nucleophilic attack by thiourea to occur only from the β face. The intermediate thiourea adduct was then converted to the thiomethyl group by exposure to methyl iodide followed by *N,N*-diisopropylethylamine (DIPEA). The order of the addition of these reagents influences the efficiency of the reaction and suggests that the methyl iodide activates the sulfur prior to the DIPEA-promoted decomposition of the thiourea intermediate. Aryl chloride **31** was coupled with methyl but-3-enoate using conditions previously reported by Fu[66] to afford the *trans* olefin **32** in 60% yield. Hydrogenation of the double bond of **32** followed by hydrolysis of the ester and acetate groups on the sugar provided acid **34**. Finally, HATU coupling of **34** with 2-amino-*N*-(2-(dimethylamino)ethyl)-2-methylpropanamide provided **21**.

Scheme 1. Synthesis of **21**[a]

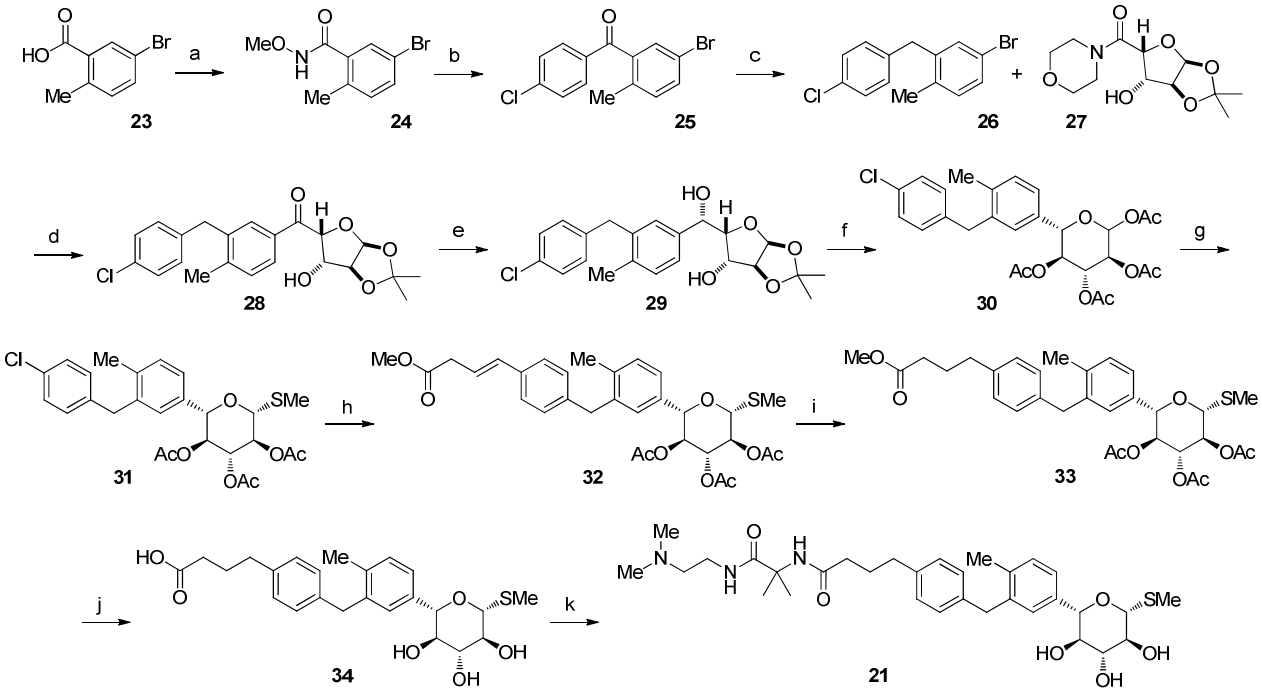

[a]Reagents and conditions: (a) $(COCl)_2$, DMF (cat.), CH_2Cl_2; MeNH(OMe)·HCl, Et_3N, CH_2Cl_2; 99% yield (b) (4-chlorophenyl)magnesium chloride, THF, 0 °C; 99% yield (c) Et_3SiH, $BF_3{\cdot}OEt_2$, CH_3CN, 60 °C; 62% yield (d) *n*-BuLi, THF, −78 °C, then **27**/*t*-BuMgCl, THF, 0 °C to 23 °C; 70% yield (e) $NaBH_4$, $CeCl_3{\cdot}7H_2O$, MeOH; 99% yield (f) HOAc/H_2O, 100 °C; Ac_2O, Et_3N, CH_3CN; 92% yield (g) TMSOTf, thiourea, dioxane, 80 °C; MeI then DIPEA, 23 °C; 60% yield (h) methyl but-3-enoate, Pd_2dba_3, [*t*-Bu_3PH]BF_4, Cy_2NMe, NMP, 160 °C, microwave irradiation; 60% yield (i) H_2, Pd/C; 94% yield (j) LiOH, MeOH/H_2O; 99% yield (k) 2-amino-*N*-(2-(dimethylamino)ethyl)-2-methylpropanamide hydrochloride, HATu, DIPEA, DMF; 40% yield after prep HPLC.

Conclusion. The discovery of preclinical candidate **21** for the selective inhibition of SGLT1 has been disclosed for the first time. **21** is a chemically stable and very potent inhibitor against SGLT1 and SGLT2 in vitro but displays specific pharmacology attributed to SGLT1 inhibition in the GI tract. We expect that this strategy could provide a promising potential therapeutic for the treatment of diabetes, particularly in patients with renal impairment who cannot benefit from the renal mechanism of selective

SGLT2 inhibitors. Further results of the pharmacology and development of this compound for therapeutic use will be reported in subsequent publications.

Experimental Section.

Chemical Methods. All reactions were conducted under a static atmosphere of argon or nitrogen and stirred magnetically unless otherwise noted. Reagents, starting materials, and solvents were purchased from commercial suppliers and used as received. Flash column chromatography was carried out using pre-packed silica gel columns from Biotage or ISCO, or by slurry preparation using EMD silica gel 60 (particle size 0.040-0.063 mm). ^{1}H and ^{13}C NMR spectra were collected on Bruker ARX300, DRX400 or DPX400 NMR spectrometers. Chemical shifts are reported in parts per million (ppm) relative to tetramethylsilane in δ-units, and coupling constants (*J*-values) are given in hertz (Hz). Data are reported in the following format: chemical shift, multiplicity, coupling constants, and assignment. Reactions were monitored by TLC using 0.25 mm E. Merck silica gel plates (60 F254) and were visualized with UV light. Analytical HPLC spectra were collected on Shimadzu HPLC systems equipped with a UV detector measuring absorbance at 220 and 254 nm. Mass spectra were obtained on Waters ZQ or ZMD LCMS systems equipped with an auto-sampler, ELSD detector, a UV detector measuring absorbance at 220 and 254 nm, and a mass detector. High resolution mass spectra were obtained on a Waters LCT Premier XE Micromass® MS Technologies instrument equipped with an auto-sampler. All compounds submitted for in vitro testing were >95% purity (HPLC) and those for in vivo testing were >98% purity (HPLC).

(5-Bromo-2-methylphenyl)(4-chlorophenyl)methanone (25). 2-Methyl-5-bromobenzoic acid (**23**, 26.0 g, 121 mmol) and oxalyl chloride (13.2 mL, 152 mmol) were suspended in 520 mL of CH_2Cl_2. A catalytic amount of DMF (0.5 mL) was added in small portions and the reaction was stirred at room temperature until the reaction became homogenous. The volatiles were removed in vacuo. The crude material was dissolved in 200 mL of CH_2Cl_2 and *N,O*-dimethylhydroxylamine hydrochloride (23.6 g, 242 mmol) was added. The reaction was cooled to 0 °C and triethylamine (55 mL, 399 mmol) was slowly

added. Upon completion of addition of triethylamine, the reaction was warmed to room temperature and stirred overnight. The reaction was quenched with 50% saturated aqueous $NaHSO_4$. The aqueous layer was extracted twice with CH_2Cl_2. The combined organic layers were washed with brine, dried over Na_2SO_4, filtered, and the solvent removed in vacuo. The resulting Weinreb amide (**24**, 31.3 g, 99% yield) was used without further purification in the next step.

The Weinreb amide (**24**, 31.3g, 121 mmol) was taken up in 250 mL of dry THF. 4-Chloromagnesium bromide (1M in Et_2O, 182 mL, 182 mmol) was added at room temperature, and the reaction stirred for 2 hours. If the reaction was not complete, additional Grignard reagent was added until LCMS indicated reaction completion. The reaction was quenched with a solution of saturated aqueous NH_4Cl/brine (1:1 v:v) and extracted twice with EtOAc. The combined organic layers were washed with brine, dried over $MgSO_4$, filtered, and the solvent removed in vacuo. (5-Bromo-2-methylphenyl)(4-chlorophenyl)methanone (**25**, 37.0 g, 99% yield) was used without further purification in the next step. ^{1}H NMR (400 MHz, CHLOROFORM-*d*) δ ppm 7.74 (d, *J*=8.3 Hz, 2 H), 7.53 (dd, *J*=8.1, 2.0 Hz, 1 H), 7.46 (d, *J*=8.3 Hz, 2 H), 7.42 (d, *J*=2.0 Hz, 1 H), 7.18 (d, *J*=8.1 Hz, 1 H), 2.26 (s, 3 H). GCMS (CH_4-CI) $[M+H]^+$ = 309.

4-Bromo-2-(4-chlorobenzyl)-1-methylbenzene (26). (5-Bromo-2-methylphenyl)(4-chlorophenyl)methanone (**25**, 37.0 g, 121 mmol) and triethylsilane (77.3 mL, 484 mmol) were dissolved in 300 mL of CH_3CN and cooled to 0 °C. $BF_3.OEt_2$ (91 mL, 726 mmol) was added and the reaction was heated to 60 °C for 2 hours. GCMS was used to monitor the reaction. Upon completion, the reaction was cooled to 0 °C and quenched with 500 mL saturated aqueous $NaHCO_3$. The aqueous phase was extracted twice with EtOAc. The combined organic layers were washed with H_2O and brine, dried over Na_2SO_4, filtered, and the solvent removed in vacuo. The crude solid was slurried in 20% EtOAc/hexanes and passed over a silica plug to remove residual salts. Concentration of the filtrate provided the title compound as a white solid (22.0 g, 62% yield). ^{1}H NMR (400 MHz, CHLOROFORM-*d*) δ ppm 7.22 (d, *J*=2.0 Hz, 1 H), 7.21 - 7.31 (m, 2 H), 7.04 (d, *J*=8.3 Hz, 2 H), 7.04 (d, *J*=8.1 Hz, 2 H), 3.91 (s, 2 H), 2.17 (s, 3 H). GCMS (CH_4-CI) $[M+H]^+$ = 295.

(3-(4-Chlorobenzyl)-4-methylphenyl)((3aS,5R,6S,6aS)-6-hydroxy-2,2-dimethyltetrahydrofuro[2,3-d][1,3]dioxol-5-yl)methanone (28). To a solution of ((3aS,5R,6S,6aS)-6-hydroxy-2,2-dimethyltetrahydrofuro[2,3-d][1,3]dioxol-5-yl)(morpholino)methanone (**27**, 25.3 g, 92.6 mmol) in THF (200 mL) under nitrogen at 0 °C was added tert-butylmagnesium chloride (1 M in THF, 100 mL, 100 mmol). This solution was stirred at 0 °C for 30 minutes. Meanwhile, a solution of 4-bromo-2-(4-chlorobenzyl)-1-methylbenzene (**26**, 32.9 g, 111.1 mmol) in THF (330 mL) under nitrogen was cooled to -78 °C. n-Butyllithium (2.5 M in hexanes, 48 mL, 120 mmol) was added dropwise via syringe and stirred for 10 min. The magnesium alkoxide solution was transferred via cannula into the aryllithium solution at -78 °C. The reaction was stirred for 30 min at -78 °C, allowed to warm to room temperature and stirred for 60 min, quenched with 500 mL of a 1:1 (v:v) solution of saturated aqueous NH_4Cl/brine. The aqueous layer was extracted two times with 300 mL of EtOAc. The combined organic layers were washed with brine, dried over $MgSO_4$, filtered, and concentrated under vacuum. The crude residue was taken up in 100 mL of EtOAc and heated until most of the solids dissolved. Hexanes (250 mL) was added and the flask was chilled in an ice bath for two hours. The white precipitate was filtered off and washed with 20% EtOAc/hexane, providing the title compound as a white solid (26.09 g, 70% yield). ^{1}H NMR (400 MHz, CHLOROFORM-*d*) δ ppm 7.88 (dd, *J*=7.8, 1.8 Hz, 1 H), 7.76 (d, *J*=1.5 Hz, 1 H), 7.29 (d, *J*=8.1 Hz, 1 H), 7.26 (d, *J*=8.3 Hz, 2 H), 7.05 (d, *J*=8.3 Hz, 2 H), 6.08 (d, *J*=3.8 Hz, 1 H), 5.28 (d, *J*=2.8 Hz, 1 H), 4.59 (d, *J*=3.5 Hz, 1 H), 4.57 (t, *J*=3.2 Hz, 1 H), 4.01 (s, 2 H), 3.06 (d, *J*=4.0 Hz, 1 H), 2.30 (s, 3 H), 1.46, (s, 3 H), 1.37 (s, 3 H). MS (ES+) $[M+H]^+$ = 403.

(3aS,5S,6R,6aS)-5-((S)-(3-(4-Chlorobenzyl)-4-methylphenyl)(hydroxy)-methyl)-2,2-dimethyltetrahydrofuro[2,3-d][1,3]dioxol-6-ol (29). (3-(4-Chlorobenzyl)-4-methylphenyl)((3aS,5R,6S,6aS)-6-hydroxy-2,2-dimethyltetrahydrofuro[2,3-d][1,3]dioxol-5-yl)methanone (**28**, 26.1 g, 64.9 mmol) and $CeCl_3 \cdot 7H_2O$ (29.0 g, 77.9 mmol) were suspended in 520 mL of MeOH. Sodium borohydride (982 mg, 26.0 mmol, dissolved in 10 mL of 1N aqueous NaOH) was added and the reactants slowly went into solution over about 5 minutes. Another 100 mg (2.6 mmol) of sodium

borohydride was added to push the reaction to completion. The reaction was stirred for 10 minutes and quenched with 500 mL of saturated aqueous NH_4Cl. Most of the MeOH was removed in vacuo and the residual solvents were diluted with a 1:1 (v:v) solution of saturated aqueous NH_4Cl:brine. The aqueous layer was extracted three times with 500 mL of EtOAc. The combined organic layers were washed with brine, dried over $MgSO_4$, filtered, and concentrated under vacuum. The crude product was used without further purification in the next step (26.2 g, 99% yield, >10:1 d.r.). ^{1}H NMR (400 MHz, CHLOROFORM-*d*) δ ppm 7.14 - 7.31 (m, 5 H), 7.04 (d, *J*=8.3 Hz, 2 H), 6.04 (d, *J*=3.8 Hz, 1 H), 5.24 (t, *J*=3.4 Hz, 1 H), 4.51 (d, *J*=3.8 Hz, 1 H), 4.14 - 4.21 (m, 2 H), 4.04 (d, *J*=1.5 Hz, 1 H), 3.97 (s, 2 H), 2.77 (d, *J*=3.0 Hz, 1 H), 2.20 - 2.27 (m, 3 H), 1.46 (s, 3 H), 1.33 (s, 3 H). MS (ES+) $[M+NH_4]^+$ = 422.

(3S,4R,5S,6S)-6-(3-(4-Chlorobenzyl)-4-methylphenyl)tetrahydro-2H-pyran-2,3,4,5-tetrayl tetraacetate (30). (3aS,5S,6R,6aS)-5-((S)-(3-(4-Chlorobenzyl)-4-methylphenyl)(hydroxy)-methyl)-2,2-dimethyltetrahydrofuro[2,3-d][1,3]dioxol-6-ol (**29**, 26.2 g, 64.8 mmol) was suspended in 150 mL H_2O and 150 mL glacial acetic acid. The reaction was heated to 100 °C for 7 hours. The solvents were removed in vacuo and the crude residue was azeotroped three times from toluene. The crude material was placed on the high vacuum overnight and used in the next step without further purification. The crude material was dissolved in 350 mL of CH_3CN. Triethylamine (57.5 mL, 414 mmol) and acetic anhydride (46.0 mL, 414 mmol) were added, followed by a catalytic amount of DMAP (100 mg). The reaction was stirred at room temperature for 1 hour. About 200 mL of CH_3CN was removed in vacuo and the remainder was diluted with 600 mL of EtOAc. The organic layer was washed twice with 50% saturated aqueous $NaHSO_4$. The acidic aqueous layers were backextracted with 300 mL of EtOAc. The combined organic layers were washed with brine, dried over $MgSO_4$, filtered, and concentrated under vacuum. The crude residue was azeotroped twice from toluene and once from hexanes to provide the title compound as an easily transferable beige solid (34.0 g, 92% yield, mixture of α and β anomers). ^{1}H NMR (400 MHz, CHLOROFORM-*d*) δ ppm 7.24 (d, *J*=8.3 Hz, 2 H), 7.13 - 7.21 (m, 2H), 7.09 (s, 1 H), 7.01 (d, *J*=8.3 Hz, 2 H), 6.47 (d, *J*=3.5 Hz, 1 Ha), 5.89 (d, *J*=8.3 Hz, 1 Hb), 5.59 (t, *J*=9.8 Hz, 1 Ha), 5.37 (t, *J*=9.6 Hz, 1 Hb), 5.23 - 5.31 (m, 1 Ha + 1 Hb), 5.19 (t, *J*=9.6 Hz, 1 Hb), 5.14 (t, *J*=9.7 Hz, 1 Ha), 4.82 (d, *J*=10.1 Hz,

1 Ha), 4.51 (d, *J*=9.9 Hz, 1 Hb), 3.94 (s, 2 H), 2.21 (s, 3 Ha), 2.20 (s, 3 Ha), 2.19 (s, 3 Hb), 2.11 (s, 3 Hb), 2.07 (s, 3 Hb), 2.06 (s, 3 Ha), 2.04 (s, 3 Ha), 2.03 (s, 3 Hb), 1.79 (s, 3 Ha), 1.77 (s, 3 Hb). MS (ES+) $[M+NH_4]^+$ = 550.

(2S,3S,4R,5S,6R)-2-(3-(4-Chlorobenzyl)-4-methylphenyl)-6-(methylthio)tetrahydro-2H-pyran-3,4,5-triyl triacetate (31). Trimethylsilyl trifluoromethanesulfonate (19.7 mL, 108.5 mmol) was added to a solution of (3S,4R,5S,6S)-6-(3-(4-chlorobenzyl)-4-methylphenyl)tetrahydro-2H-pyran-2,3,4,5-tetrayl tetraacetate (**30**, 33.9 g, 63.8 mmol) and thiourea (9.71 g, 128 mmol) in 340 mL of dioxane. The reaction was heated to 80 °C for two hours, at which point LCMS analysis revealed the reaction was stalled. Additional TMSOTf was added (2 mL, 10.8 mmol) and the reaction stirred for 1 hour at 80°C. The reaction was cooled to room temperature. Sequential addition of methyl iodide (11.9 mL, 191 mmol) followed by DIPEA (55.6 mL, 319 mmol) was performed, allowing the reaction to stir for 18 hours. 500 mL of H_2O was slowly added to quench the reaction. The aqueous layer was extracted two times with 300 mL EtOAc. The combined organic layers were washed with saturated aqueous $NaHSO_4$ and brine, dried over $MgSO_4$, filtered, and concentrated under vacuum. The crude solid was slurried in 300 mL of MeOH. Sonication resulted in the precipitation of a light beige precipitate, which was filtered and washed with cold MeOH. The filtrate was concentrated and the slurry procedure repeated once more to provide and combined with the first batch. The product was isolated as pure beta anomer as a light beige solid (20.4 g, 60% yield). ^{1}H NMR (400 MHz, CHLOROFORM-*d*) δ ppm 7.24 (d, *J*=8.6 Hz, 2 H), 7.10 - 7.18 (m, 2 H), 7.05 (s, 1 H), 7.00 (d, *J*=8.6 Hz, 2 H), 5.34 (dd, *J*=9.6 Hz, 1 H), 5.21 (dd, *J*=9.6 Hz, 1 H), 5.12 (dd, *J*=9.6 Hz, 1 H), 4.53 (d, *J*=9.9 Hz, 1 H), 4.39 (d, *J*=9.9 Hz, 1 H), 3.86 - 4.00 (m, 2 H), 2.19 (s, 3 H), 2.17 (s, 3 H), 2.10 (s, 3 H), 2.01 (s, 3 H), 1.76 (s, 3 H). MS (ES+) $[M+NH_4]^+$ = 538.

(2S,3S,4R,5S,6R)-2-(3-(4-((E)-4-Methoxy-4-oxobut-1-en-1-yl)benzyl)-4-methylphenyl)-6-(methylthio)tetrahydro-2H-pyran-3,4,5-triyl triacetate (32). A microwave vial was charged with (2S,3S,4R,5S,6R)-2-(3-(4-chlorobenzyl)-4-methylphenyl)-6-(methylthio)tetrahydro-2H-pyran-3,4,5-triyl triacetate (**31**, 1.04 g, 2.0 mmol), methyl but-3-enoate (600 mg, 6.0 mmol), Pd_2dba_3 (183 mg, 0.20 mmol), tri(tert-butyl)phosphonium tetrafluoroborate (235 mg, 0.80 mmol), dicyclohexylmethylamine (1.27 mL,

6.0 mmol), and *N*-methylpyrrolidinone (10 mL). The reaction was heated in the microwave at 160 °C for 20 min. The reaction was filtered over Celite with excess EtOAc. The organic layer was washed with H_2O, saturated aqueous $NaHSO_4$, and brine. It was dried with $MgSO_4$ and concentrated in vacuo. Silica gel flash chromatography (gradient 10-50% EtOAc/hexanes) provided Heck adduct **32** as a light yellow solid (700 mg, 60% yield). Minor amounts of isomerized olefin were observed in the ^{1}H NMR. ^{1}H NMR (400 MHz, CHLOROFORM-*d*) δ ppm 7.28 - 7.31 (m, 2 H), 6.97 - 7.19 (m, 5 H), 6.46 (d, *J*=15.9 Hz, 1 H), 6.25 (dt, *J*=15.9, 7.1 Hz, 1 H), 5.33 (dd, *J*=9.6 Hz, 1 H), 5.21 (dd, *J*=9.6 Hz, 1 H), 5.12 (dd, *J*=9.6 Hz, 1 H), 4.52 (d, *J*=9.6 Hz, 1 H), 4.39 (d, *J*=9.6 Hz, 1 H), 3.87 - 4.01 (m, 2 H), 3.72 (s, 3 H), 3.24 (dd, *J*=7.1, 1.3 Hz, 2 H), 2.21 (s, 3 H), 2.17 (s, 3 H), 2.10 (s, 3 H), 2.01 (s, 3 H), 1.75 (s, 3 H). MS (ES+) $[M+NH_4]^+$ = 602.

(2S,3S,4R,5S,6R)-2-(3-(4-(4-Methoxy-4-oxobutyl)benzyl)-4-methylphenyl)-6-(methylthio)tetrahydro-2H-pyran-3,4,5-triyl triacetate (33). (2S,3S,4R,5S,6R)-2-(3-(4-((E)-4-Methoxy-4-oxobut-1-en-1-yl)benzyl)-4-methylphenyl)-6-(methylthio)tetrahydro-2H-pyran-3,4,5-triyl triacetate (**32**, 1.74 g, 3.0 mmol) was dissolved in a 1:1 (v:v) THF/MeOH solution. Pd/C (10% wet, 174 mg) was added and the reaction hydrogenated at 40 psi for 3 hours. The reaction was monitored by ^{1}H NMR. Upon completion, the reaction was filtered over Celite with excess MeOH. Removal of solvents in vacuo provided the product as a light yellow solid (1.65 g, 94% yield). ^{1}H NMR (400 MHz, CHLOROFORM-*d*) δ ppm 7.11 - 7.20 (m, 2 H), 7.07 (t, *J*=7.8 Hz, 3 H), 6.99 (d, *J*=8.1 Hz, 2 H), 5.33 (dd, *J*=9.6 Hz, 1 H), 5.21 (dd, *J*=9.6 Hz, 1 H), 5.12 (dd, *J*=9.6 Hz, 1 H), 4.52 (d, *J*=9.9 Hz, 1 H), 4.39 (d, *J*=9.9 Hz, 1 H), 3.85 - 4.00 (m, 2 H), 3.67 (s, 3 H), 2.61 (t, *J*=7.6 Hz, 2 H), 2.33 (t, *J*=7.5 Hz, 2 H), 2.21 (s, 3 H), 2.18 (s, 3 H), 2.10 (s, 3 H), 2.01 (s, 3 H), 1.93 (quin, *J*=7.6 Hz, 2 H), 1.75 (s, 3 H). MS (ES+) $[M+NH_4]^+$ = 604.

4-(4-(2-Methyl-5-((2S,3R,4R,5S,6R)-3,4,5-trihydroxy-6-(methylthio)tetrahydro-2H-pyran-2-yl)benzyl)phenyl)butanoic acid (34). (2S,3S,4R,5S,6R)-2-(3-(4-(4-Methoxy-4-oxobutyl)benzyl)-4-methylphenyl)-6-(methylthio)tetrahydro-2H-pyran-3,4,5-triyl triacetate (**33**, 1.65 g, 2.81 mmol) was dissolved in a MeOH/THF/H_2O solution (25 mL, 2:1:2 vol. ratio). Lithium hydroxide (674 mg, 28.1

mmol) was added and the reaction stirred at room temperature for 1 hour. The reaction was acidified to pH = 1-2 with saturated aqueous $NaHSO_4$. The acidic aqueous layer was extracted three times with EtOAc. The combined organic layers were washed with brine, dried over $MgSO_4$, filtered, and concentrated in vacuo. The crude product was rotovapped down once from hexanes to provide the product as white transferrable solid (1.27 g, 99% yield). ^{1}H NMR (400 MHz, DMSO-d_6) δ ppm 11.99 (s, 1 H), 6.96 - 7.16 (m, 7 H), 4.39 (d, J=9.6 Hz, 1 H), 4.12 (d, J=9.1 Hz, 1 H), 3.90 (s, 2 H), 3.34 —3.51 (m, 3 H), 2.53 (t, *J*=7.3 Hz, 2 H), 2.19 (t, *J*=7.3 Hz, 2 H), 2.17 (s, 3 H), 2.03 (s, 3 H), 1.76 (quin, *J*=7.6 Hz, 2 H). MS (ES+) $[M+NH_4]^+$ = 464.

N-(1-((2-(dimethylamino)ethyl)amino)-2-methyl-1-oxopropan-2-yl)-4-(4-(2-methyl-5-((2S,3R,4R,5S,6R)-3,4,5-trihydroxy-6-(methylthio)tetrahydro-2H-pyran-2-yl)benzyl)phenyl)butanamide (21). 4-(4-(2-Methyl-5-((2S,3R,4R,5S,6R)-3,4,5-trihydroxy-6-(methylthio)tetrahydro-2H-pyran-2-yl)benzyl)phenyl) butanoic acid (**34**, 157 mg, 0.35 mmol), 2-amino-*N*-(2-(dimethylamino)ethyl)-2-methylpropanamide hydrochloride (73 mg, 0.53 mmol), HATU (161 mg, 0.42 mmol), and DIPEA (0.15 mL, 1.06 mmol) were combined in DMF (2 mL) and stirred for 2 hours at room temperature. The reaction was quenched with saturated aqueous $NaHCO_3$ and extracted twice with EtOAc. The combined organic layers were washed with brine, dried with $MgSO_4$, filtered, and concentrated under vacuum. The residue was purified by preparative HPLC (C18 30 x 100 mm column, 5-100% CH_3CN/10 mM aqueous ammonium formate, 45 mL/min) to provide the title compound **21** as the formate salt after lyophilization (75 mg, 40% yield). ^{1}H NMR (400 MHz, MeOH-d_4) δ ppm 8.52 (s, 1 H), 7.12 - 7.21 (m, 3 H), 7.03 - 7.12 (m, 4 H), 4.39 (d, *J*=9.6 Hz, 1 H), 4.13 (d, *J*=9.3 Hz, 1 H), 3.96 (s, 2 H), 3.51 (t, *J*=5.6 Hz, 2 H), 3.33 - 3.47 (m, 3 H), 3.07 (t, *J*=4.8 Hz, 2 H), 2.79 (s, 6 H), 2.60 (t, *J*=7.6 Hz, 2 H), 2.21 (s, 3 H), 2.22 (t, *J*=7.6 Hz, 2 H), 2.14 (s, 3 H), 1.88 (quin, *J*=7.5 Hz, 2 H), 1.41 (s, 6 H). MS (ES+) $[M+H]^+$ = 602.

Biological Methods (In Vitro). *Human SGLT1 Inhibition Assay.* Human sodium/glucose co-transporter type 1 (SGLT1; accession number NP_000334; GI: 4507031) was cloned into pIRESpuro2 vector for mammalian expression (construct: HA-SGLT1-pIRESpuro2). HEK293 cells were transfected

with the human HA-SGLT1-pIRESpuro2 vector and the stably transfected cell line was established in the presence of 0.5 μg/mL of puromycin. Human HA-SGLT1 cells were maintained in DMEM media containing 10% fetal bovine serum, 2 M L-glutamine, 100 units penicllin/mL, 0.1 mg/mL streptomycin, and 0.5 μg/mL puromycin. The HEK293 cells expressing the human HA-SGLT1 were seeded in 384 well plates (30,000 cells/well) in DMEM media containing 10% fetal bovine serum, 2 M L-glutamine, 100 units penicllin/mL, 0.1 mg/mL streptomycin, and 0.5 μg/mL puromycin, then incubated overnight at 37 °C, 5% CO_2. Cells were then washed with uptake buffer (140 mM NaCl, 2 mM KCl, 1 mM $CaCl_2$, 1 mM $MgCl_2$, 10 mM HEPES, 5 mM Tris, 1 mg/mL bovine serum albumin (BSA), pH 7.3). Twenty microliters of uptake buffer with or without testing compounds were added to the cells. Then, 20 microliters of uptake buffer containing ^{14}C-AMG (100 nCi) were also added to cells. The cell plates were incubated at 37 °C, 5% CO_2 for 1-2 hours. After washing the cells with uptake buffer, scintillation fluid was added (40 microliters/well) and ^{14}C-AMG uptake was measured by counting radioactivity using a scintillation coulter (TopCoulter NXT; Packard Instruments). The calculation of the IC_{50} is performed using XLFit4 software, Model 205 (ID Business Solutions Inc., Bridgewater, NJ 08807) for Microsoft Excel.

Human SGLT2 Inhibition Assay. Human sodium/glucose co-transporter type 2 (SGLT2; accession number P31639; GI:400337) was cloned into pIRESpuro2 vector for mammalian expression (construct: HA-SGLT2-pIRESpuro2). HEK293 cells were transfected with the human HA-SGLT2-pIRESpuro2 vector and the stably transfected cell line was established in the presence of 0.5 μg/mL of puromycin. Human HA-SGLT2 cells were maintained in DMEM media containing 10% fetal bovine serum, 2 M L-glutamine, 100 units penicllin/mL, 0.1 mg/mL streptomycin, and 0.5 μg/mL puromycin. The HEK293 cells expressing the human HA-SGLT2 were seeded in 384 well plates (30,000 cells/well) in DMEM media containing 10% fetal bovine serum, 2 M L-glutamine, 100 units penicllin/mL, 0.1 mg/mL streptomycin, and 0.5 μg/mL puromycin, then incubated overnight at 37 °C, 5% CO_2. Cells were then washed with uptake buffer (140 mM NaCl, 2 mM KCl, 1

mM $CaCl_2$, 1 mM $MgCl_2$, 10 mM HEPES, 5 mM Tris, 1 mg/mL bovine serum albumin (BSA), pH 7.3). Twenty microliters of uptake buffer with or without testing compounds were added to the cells. Then, 20 microliters of uptake buffer containing ^{14}C-AMG (100 nCi) were added to the cells. The cell plates were incubated at 37°C, 5% CO_2 for 1-2 hours. After washing the cells with uptake buffer, scintillation fluid was added (40 microliters/well) and ^{14}C-AMG uptake was measured by counting radioactivity using a scintillation coulter (TopCoulter NXT; Packard Instruments). The calculation of the IC_{50} is performed using XLFit4 software, Model 205 for Microsoft Excel.

Biological Methods (In Vivo). All studies were performed at Lexicon Pharmaceuticals, Inc., in strict accordance with the recommendations in the Guide for the Care and Use of Laboratory Animals of the National Institutes of Health. The protocols for all studies were approved by the Lexicon Institutional Animal Care and Use Committee (OLAW Assurance Number, A4152-01; AAALAC International Accreditation Number, 001025). General methods for mouse care have been described by us previously.[40,59] C57BL/6-*Tyr*c-Brd (C57) mice obtained from an in-house colony were fed either standard rodent chow diet (5010, LabDiet, PMI Nutrition International, St. Louis, MO) containing 23% calories as fat or low fat diet (LFD; D12451, Research Diets, New Brunswick, NJ) containing 10% calories as lard fat and 35% calories as sucrose. Mice were maintained in a temperature-controlled environment on a fixed 12 hour light/12 hour dark cycle and with free access to water and food. In all in vivo studies presented here, all compounds were administered by oral gavage in a volume of no more than 10 mL/kg, and the vehicle was always aqueous 0.1% v/v Tween 80.

Urinary Glucose Excretion Study in C57 Mice. At 15 weeks of age, male C57 mice were individually housed in metabolic cages (Nalge Nunc International, Rochester, NY) and fed powdered low-fat diet (LFD, 10% lard fat, 35% sucrose) homogenized in water at a 2:1 (wt:wt) ratio. This paste diet prevented contamination of urine with crumbled diet. After an acclimatization period, each mouse received, by oral gavage, a single dose of either vehicle or vehicle containing either 21 or 1. Complete 24-hour urine samples were collected during the 24 hours after dosing (day 1) and also on day 2. After the volume of each 24-hour urine collection was recorded, the urine sample was centrifuged and analyzed

for glucose concentration (Cobas Integra 400 Clinical Chemistry Autoanalyzer, Roche Diagnostics, Indianapolis, IN).

Glucose-containing Meal Challenge Study in C57 Mice. LFD-fed, adult male C57 mice were randomized into treatment groups by body weight. Each mouse received either vehicle or 21 by oral gavage and then, 22 hours later after a 16 hour fast, received a meal consisting of LFD supplemented with glucose. This meal was prepared, as described previously[41]: 50 g of LFD powder and 9.4 g of glucose were added to water at 60 °C; the final volume was 94 mL and the meal was kept until used. The mice received 25 ml/kg of this meal (9.2 g/kg glucose, 2.5 g/kg protein, 0.6 g/kg fat) by oral gavage. Blood samples were collected through retro-orbital bleeding at 0, 10, 30 and 60 minutes after meal challenge for assessment of glucose excursion. In addition, blood samples collected 60 minutes after meal challenge were used to measure circulating levels of total glucagon-like peptide 1 (tGLP-1). Mice were necropsied at the end of the meal challenge (23 hours after the dose of compound or vehicle) and cecal contents were collected, weighed and frozen at -20 °C for later analysis. For batched analysis, samples were thawed on wet ice, and MilliQ water was added to each sample at the ratio (w/v) of 1:5. The samples were then homogenized by bead-beating using a Mini Beadbeater (Biospec Products) at high speed for one minute. The homogenized samples were centrifuged at 4 °C at 3750 rpm (3200 *g*) for 25 minutes. The supernatant was removed and the volume was recorded. A 25 µL aliquot of supernatant was assayed for glucose concentration by Roche Cobas Integra 400 Clinical Chemistry Autoanalyzer. Total glucose content (mg) was estimated by multiplying the glucose concentration by the volume of the centrifuged supernatant. The remaining supernatant was thawed to room temperature for pH measurement, which was performed using a Mettler Toledo FE20 pH Meter.

Analysis of Blood Samples. Whole blood glucose was measured using an Accu-Chek Aviva glucometer (Roche Diagnostics, Indianapolis, IN). Plasma GLP-1 levels were measured using the Glucagon-Like Peptide-1 Total ELISA Kit (catalog #EZGLP1T-36K, Millipore, St. Charles, MO) exactly as described previously.[41]

Pharmacokinetics and Data Analysis. Adult male C57 mice (25-35 g) were maintained on chow diet with free access to water and were conscious throughout the study. For bolus intravenous administration (IV), 21 and 1 were dissolved in 0.1% Tween-80 to form a clear solution and was then administered at a dose of 1 mg/kg. For oral administration, 21 was provided by gavage at a dose of 10 mg/kg or 30 mg/kg, while 1 was provided by gavage at a dose of 30 mg/kg. Following intravenous injection, serial blood samples were collected in EDTA-containing tubes through 6 hours, and following oral administration, serial blood samples were collected through 24 hours. The plasma fraction was immediately separated by centrifugation at 4 ^{o}C, and then stored at -20 ^{o}C until sample analysis. Bioanalysis of plasma samples for quantitating plasma concentrations of compounds **21** and **1** was conducted using liquid chromatography/mass spectroscopy. All plasma concentration versus time data for **21** were analyzed using non-compartmental model 200 (for oral administration) and 201 (for IV administration) of WinNonlin (version 5.0, Pharsight, Inc. Mountain View, CA) as described previously.[59] The half-life during the terminal phase was calculated from the elimination rate constant (λ) determined by the linear regression analysis of the log-linear part of the plasma concentration curve. The $AUC_{0\text{-}t}$ was calculated using linear up/log down trapezoidal method up to the last measured concentration at time t. $AUC_{0\text{-}\infty}$ was calculated as $AUC_{0\text{-}t} + C_t/\lambda$. Clearance (CL) was calculated by dose/$AUC_{0\text{-}\infty}$. Other pharmacokinetic parameters included plasma peak concentration (C_{max}), the time of C_{max} (T_{max}) and volume of distribution at steady state (V_{ss}).

Associated Content

Supporting Information. **S**ynthetic methods and characterization for compounds in Tables 1 and 2. The Supporting Information is available free of charge on the ACS Publications website.

Author Information

Corresponding Author.

*(NCG) Current address: GlaxoSmithKline, 709 Swedeland Rd, King of Prussia, PA 19406. E-mail: nicole.c.goodwin@gsk.com. Tel: +1 (610) 270-4260

Notes. All authors contributed equally to this work. D.R.P., S.G., and A.G.E.W are current employees of Lexicon Pharmaceuticals and own stock. N.C.G., Z.M.D., B.A.H., A.L.H., M.S., A.Y.T., W.X., F.M., D.J.B, E.O., M.T., R.B.V., and D.B.R. were employees of Lexicon Pharmaceuticals at the time of studies and own stock. E.D.S., D.D., L.L., E.O., and K.G.C. were employees of Lexicon Pharmaceuticals at the time of the study and declare no competing interests. The authors wish to acknowledge Kristi Boehm, MS, ELS for her help in figure preparation.

Abbreviations Used

SGLT, sodium-dependent glucose cotransporter; GI, gastrointestinal; GGM, glucose-galactose malabsorption; KO, knock-out; FDA, Food & Drug Administration; UGE, urinary glucose excretion; PPG, postprandial glucose; GLP-1, glucagon-like peptide 1; tGLP-1, total GLP-1; SAR, structure-activity relationship; AMG, alpha-methylglucopyranoside; IC_{50}, half maximal (50%) inhibitory concentration; mSGLT, mouse SGLT; hSGLT, human SGLT; DIO, diet-induced obese; OGTT, oral glucose tolerance test; NMR, nuclear magnetic resonance; HCl, hydrochloric acid; PK, pharmacokinetic; $BF_3{\cdot}OEt_2$, boron trifluoride diethyl etherate; TMSOTf, trimethylsilyl trifluoromethanesulfonate; DIPEA, *N,N*-diisopropylethylamine; HATU, 1-[bis(dimethylamino)methylene]-1H-1,2,3-triazolo[4,5-b]pyridinium 3-oxid hexafluorophosphate

References

(1) Diabetes Fact Sheet, www.who.int/mediacentre/factsheets/fs312/en; accessed March 6, 2016.

(2) Fowler, M. J. Microvascular and Macrovascular Complications of Diabetes. *Clin. Diabetes* **2008**, *26*, 77-82.

(3) Morrish, N .J.; Wang, S. L.; Stevens, L. K.; Fuller, J. H.; Keen, H. Mortality and Causes of Death in the WHO Multinational Study of Vascular Disease in Diabetes. *Diabetologia* **2001**, *44*, S14-S21.

(4) Tancredi, M.; Rosengren, A.; Svensson, A. M.; Kosiborod, M.; Pivodic, A.; Gudbjornsdottir, S.; Wedel, H.; Clements, M.; Dahlqvist, S.; Lind, M. Excess Mortality Among Persons with Type 2 Diabetes. *N. Eng. J. Med.* **2015**, *373*, 1720-1732.

(5) Mudaliar, S.; Polidori, D.; Zambrowicz, B.; Henry, R. R. Sodium-Glucose Cotransporter Inhibitors: Effects on Renal and Intestinal Glucose Transport: From Bench to Bedside. *Diabetes Care* **2015**, *38*, 2344-2353.

(6) Marsenic, O. Glucose Control by the Kidney: an Emerging Target in Diabetes. *Am. J. Kidney Dis.* **2009**, *53*, 875-883.

(7) Wright, E. M. Renal Na+-Glucose Cotransporters. *Am. J. Physiol. Renal. Physiol.* **2001**, *280*, F10-F18.

(8) Nishimura, M.; Naito, S. Tissue-specific mRNA Expression Profiles of Human ATP-binding Cassette and Solute Carrier Transporter Superfamilies. *Drug Metab. Pharmacokinet.* **2005**, *20*, 452-477.

(9) Turk, E.; Zwbel, B.; Mundlos, S.; Dyer, J.; Wright, E. M. Glucose/galactose Malabsorption Caused by a Defect in the Na+/glucose Cotransporter. *Nature* **1991**, *350*, 354-356.

(10) Martin, M. G.; Turk, E.; Lostao, M. P.; Kerner, C.; Wright, W. M. Defects in Na^+/glucose Cotransporter (SGLT1) Trafficking and Function Cause Glucose-galactose Malabsorption. *Nat. Genet.* **1996**, *12*, 216-220.

(11) Kanai, Y.; Lee, W. S.; You, G.; Brown, D.; Hediger, M. A. The Human Kidney Low Affinity Na^+/glucose Cotransporter SGLT2: Delineation of the Major Renal Reabsorptive Mechanism for D-glucose. *J. Clin. Invest.* **1994**, *93*, 397-404.

(12) Van den Heuvel, L. P.; Assink, K.; Willemsen, M.; Monnens, L. Autosomal Recessive Renal Glucosuria Attributable to a Mutation in the Sodium Glucose Cotransporter (SGLT2). *Hum. Genet.* **2002**, *111*, 544-547.

(13) Santer, R.; Calado, J. Familial Renal Glucosuria and SGLT2: From a Mendelian Trait to a Therapeutic Target. *Clin. J. Am. Soc. Nephrol.* **2010**, *5*, 133-141.

(14) Lam, J. T.; Martin, M. G.; Turk, E.; Hirayama, B.A.; Bosshard, N. U.; Steinmann, B,; Wright, E. M. Missense Mutations in SGLT1 Cause Glucose-galactose Malabsorpion by Trafficking Defects. *Biochim. Biophys. Acta* **1999**, *1453*, 297-303.

(15) Gorboulev, V.; Schurmann, A,; Vallon, V.; Kipp, H.; Jaschke, A.; Klessen, D.; Friedrich, A.; Scherneck, S.; Rieg, T.; Cunard, R.; Veyhl-Wichmann, M.; Srinivasan, A.; Balen, D.; Breljak, D.; Rexhepal, R.; Parker, H. E.; Gribble, F. M.; Reiman, F.; Lang, F.; Wiese, S.; Sabolic, I.; Sendtner, M.; Koepsell, H. Na(+)-D-glucose Cotransporter SGLT1 is Pivotal for Intestinal Glucose Absorption and Glucose-dependent Incretin Secretion. *Diabetes* **2012**, *61*, 187-196.

(16) Wright, E. M.; Turk, E.; Martin, M. G. Molecular Basis for Glucose-galactose Malabsorption. *Cell Biochem. Biophys.* **2002**, *36*, 115-121.

(17) Xin, B.; Wang, H. Multiple Sequence Variations in *SLC5A1*G are Associated with Glucose-galactose Malabsorption in Large Cohort of Old Order Amish. *Clin. Genet.* **2011**, *79*, 86-91.

(18) Washburn, W. N. Development of the Renal Glucose Reabsorption Inhibitors: a New Mechanism for the Pharmacotherapy of Diabetes Mellitus Type 2. *J. Med. Chem.* **2009**, *52*, 1785-1794.

(19) Washburn, W. N. Evolution of Sodium Glucose Co-Transporter 2 Inhibitors as Anti-Diabetic Agents. *Expert Opin. Ther. Pat.* **2009**, *19*, 1485-1499.

(20) Meng, W.; Ellsworth, B. A.; Nirschl, A. A.; McCann, P. J.; Patel, M.; Girotra, R. N.; Wu, G.; Sher, P. M.; Morrison, E. P.; Biller, S. A.; Zahler, R.; Deshpande, P. P.; Pullockaran, A.; Hagan, D. L.; Morgan, N.; Taylor, J. R.; Obermeier, M. T.; Humphreys, W. G.; Khanna, A.; Discenza, L.; Robertson, J. G.; Wang, A.; Han, S.; Wetterau, J. R.; Janovitz, E. B.; Flint, O. P.; Whaley, J. M.; Washburn, W. N. Discovery of Dapagliflozin: a Potent, Selective Renal Sodium-dependent Glucose Cotransporter 2 (SGLT2) Inhibitor for the Treatment of Type 2 Diabetes. *J. Med. Chem*. **2008**, *51*, 1145–1149.

(21) Deshpande, P. P.; Ellsworth, B. A.; Singh, J.; Denzel, T. W.; Lai, C.; Chiajen, G.; Randazzo, M. E.; Gougoutas, J. Z. Methods of Producing C-Aryl Glucoside SGLT2 Inhibitors. U.S. Pat. Appl. Pub. US2004138439, 2004.

(22) List, J. F.; Woo, V.; Morales, E.; Tang, W.; Fiedorek, F. T. Sodium-glucose Cotransport Inhibition with Dapagliflozin in Type 2 Diabetes. *Diabetes Care* **2009**, *32*, 650-657.

(23) Nomura, S.; Sakamaki, S.; Hongu, M.; Kawanishi., E.; Koga, Y.; Sakamoto, T.; Yamamoto, Y.; Ueta, K.; Kimata, H.; Nakayama, K.; Tsuda-Tsukimoto, M. Discovery of Canagliflozin, a Novel C-Glucoside with Thiophene Ring, as Sodium-Dependent Glucose Co-transporter 2 Inhibitor for the Treatment of Type 2 Diabetes Mellitus. *J. Med. Chem.* **2010**, *53*, 6355-6360.

(24) Nomura, S.; Kawanishi, E.; Ueta, K. Preparation of Glycosides as Antidiabetic Agents and Having Inhibitory Activity against Sodium- Dependent Transporter. PCT Int. Appl. WO2005012326, 2005.

(25) Abdel-Magid, A. F.; Chisholm, M.; Mehrman, S.; Scott, L.; Wells, K. M.; Zhang-Plasket, F.; Nomura, S.; Hongu, M.; Koga, Y. Process for the Preparation of Compounds Useful as Inhibitors of SGLT. PCT Int. App. WO2009035969, 2009.

(26) Meininger, G.; Canovatchel, W.; Polidori, D.; Rosenthal, N. Canagliflozin for the Treatment of Adults with Type 2 Diabetes. *Diabetes Management* **2015**, *5*, 183-201.

(27) Eckhardt, M.; Himmelsbach, F.; Wang, X.-J.; Sun, X.; Zhang, L.; Tang, W.; Krishnamurthy, D.; Senanayake, C. H.; Han, Z . Processes for the Preparation of Glucopyranosyl-substituted Benzyl or Benzene Derivatives**.** PCT Int. Appl. WO 2006120208, 2006.

(28) Neumiller, J. J.. Empagliflozin: A New Sodium-glucose Co-transporter 2 (SGLT2) Inhibitor for the Treatment of Type 2 Diabetes. *Drugs Context* **2014**, *3*, 212-262.

(29) Imamura, M.; Nakanishi, K.; Suzuki, T.; Ikegai, K.; Shiraki, R.; Ogiyama, T.; Murakami, T.; Kurosaki, E.; Noda, A.; Kobayashi, Y.; Yokota, M.; Koide, T.; Kosakai, K.; Ohkura, Y.; Takeuchi, M.; Tomiyama, H.; Ohta, M. Discovery of Ipragliflozin (ASP1941): A Novel C-Glucoside with Benzothiophene Structure as a Potent and Selective Sodium Glucose Co-transporter 2 (SGLT2) Inhibitor for the Treatment of Type 2 Diabetes Mellitus. *Bioorg. Med. Chem.* **2012**, *20*, 3263-3279.

(30) Imamura, M.; Murakami, T.; Shiraki, R.; Ikegai, K.; Sugane, T.; Iwasaki, F.; Kurosaki, E.; Tomiyama, H.; Noda, A.; Kitta, K.; Kobayashi, Y. Preparation of C-Glucoside Derivatives and Salts Therof as Na+-glucose Co-Transporter Inhibitor. PCT Int. Appl. WO 2004080990, 2004.

(31) Kadokura, T.; Zhang, W.; Krauwinkel, W.; Leeflang, S.; Keirns, J.; Taniuchi, Y.; Nakajo, I.; Smulders, R. Clinical Pharmcokinetics and Pharmadynamics of the Novel SGLT2 Inhibitor Ipragliflozin. *Clin. Pharmacokinet.* **2014**, *53*, 975-988.

(32) Kakinuma, H.; Oi, T.; Hashimoto-Tsuchiya, Y.; Arai, M.; Kawakita, Y.; Fukasawa, Y.; Iida, I.; Hagima, N.; Takeuchi, H.; Chino, Y.; Asami, J.; Okumura-Kitajima, L.; Io, F.; Yamamoto, D.; Miyata, N.; Takahashi, T.; Uchida, S.; Yamamoto, K. (1*S*)-1,5-Anhydro-1-[5-(4-ethoxybenzyl)-2-methoxy-4-methylphenyl]-1-thio-D-glucitol (TS-071) is a Potent, Selective Sodium-Dependent Glucose Cotransporter 2 (SGLT2) Inhibitor for Type 2 Diabetes Treatment. *J. Med. Chem.* **2010**, *53*, 3247-3261.

(33) Sato, M.; Kakinuma, H.; Asanuma, H. Preparation of Aryl 5-Thio-β-D-Glucopyranoside Derivatives As Remedies for Diabetes. PCT Int Appl. WO2004014931, 2004

(34) Markham, A.; Elkinson, S. Luseogliflozin: First Global Approval. *Drugs* **2014**, *74*, 945-950.

(35) Ohtake, Y.; Sato, T.; Kobayashi, T.; Nishimoto, M.; Taka, N.; Takano, K.; Yamamoto, K.; Ohmori, M.; Yamaguchi, M.; Takami, K.; Yeu, S. Y.; Ahn, K. H.; Matsuoka, H.; Morikawa, K.; Suzuki, M.; Hagita, H.; Ozawa, K.; Yamaguchi, K.; Kato, M.; Ikeda, S. Discovery of Tofogliflozin, a Novel C-Arylglucoside with an O-Spiroketal Ring System, as a Highly Selective Sodium Glucose Cotransporter 2 (SGLT2) Inhibitor for the Treatment of Type 2 Diabetes. *J. Med. Chem.* **2012***, 55*, 7828–7840.

(36) Matsuoka, H.; Sato, T.; Nishimoto, M.; Shimma, N. Preparation of Benzylphenyl-5a-carba-β-D-glucopyranoside Derivatives as Na+-glucose Cotransporter Inhibitors. PCT Int. Appl. WO2006011469, 2006.

(37) Poole, R. M.; Prossler, J. E. Tofogliflozin: First Global Approval. *Drugs* **2014**, *74*, 939-944.

(38) Zambrowicz, B. P.; Friedrich, G. A.; Buxton, E. C.; Lilleberg, S. L.; Sands, A. T. Disruption and Sequence Identification of 2000 Genes in Mouse Embryonic Stem Cells. *Nature* **1998**, *392*, 608-611.

(39) Zambrowicz, B. P.; Friedrich, G. A. Comprehensive Mammalian Genetics: History and Future of Gene Trapping in the Mouse. *Int. J. Dev. Biol.* **1998**, *42*, 1025-1036.

(40) Powell, D. R.; DaCosta, C. M.; Gay, J.; Ding, Z.-M.; Smith, M.; Greer, J.; Doree, D.; Jeter-Jones, S.; Mseeh, F.; Rodriguez, L. A.; Harris, A.; Buhring, L.; Platt, K. A.; Vogel, P.; Brommage, R.; Shadoan, M. K.; Sands, A. T.; Zambrowicz, B. P. Improved Glycemic Control in Mice Lacking SGLT1 and SGLT2. *Am. J. Physiol.* **2013**, *304*, E117-E130.

(41) Powell, D. R.; Smith, M.; Greer, J.; Harris, A.; Zhao, S.; DaCosta, C. M.; Mseeh, F.; Shadoan, M. K.; Sands, A. T.; Zambrowicz, B. P.; Ding, Z.-M. LX4211 Increases Serum Glucagon-like Peptide 1 and Peptide YY Levels by Reducing Sodium/glucose Cotransporter 1 (SGLT1)-mediated Absorption of Intestinal Glucose. *J. Pharmacol. Exp. Ther.* **2013**, *345*, 250-259.

(42) Mulvihill, E. E.; Drucker, D. J. Pharmacology, Physiology, and Mechanisms of Action of Dipeptidyl Peptidase-4 Inhibitors. *Endocrine Rev.* **2014**, *35*, 992-1019.

(43) Zambrowicz, B. P.; Freiman, J.; Brown, P. M.; Frazier, K. S.; Turnage, A.; Bronner, J.; Ruff, D.; Shadoan, M.; Banks, P.; Mseeh, F.; Rawlins, D. B.; Goodwin, N. C.; Mabon, R.; Harrison, B. A.; Wilson, A.; Sands, A.; Powell, D. R. LX4211, a Dual SGLT1/SGLT2 Inhibitors, Improved Glycemic Control in Patients With Type 2 Diabetes in a Randomized, Placebo-Controlled Trial. *Clin. Pharmacol. Ther.* **2012**, *92*, 18-169.

(44) Lapuerta, P.; Zambrowicz, B.; Strumph, P.; Sands, A. Development of Sotagliflozin, a Dual Sodium-dependent Glucose Transporter 1/2 Inhibitor. *Diabetes Vasc. Dis. Res.* **2015**, *12*, 101-110.

(45) Zambrowicz, B. P.; Ogbaa, I.; Frazier, K. S.; Banks, P.; Turnage, A.; Freiman, J.; Boehm, K.A.; Ruff, D.; Powell, D.R.; Sands, A. Effects of LX4211, a Dual Sodium-Dependent Glucose Cotransporters 1 and 2 Inhibitor, on Postprandial Glucose, Insulin, Glucagon-like Peptide 1, and Peptide Tyrosine Tyrosine in a Dose-Timing Study in Healthy Subjects. *Clin. Ther.* **2013**, *35*, 1162-1773.

(46) Zambrowicz, B. P.; Ding, Z.-M.; Ogbaa, I.; Frazier, K.; Banks, P.; Turnage, A.; Freiman, J.; Smith, M.; Ruff, D.; Sands, A. T.; Powell, D. R. Effects of LX4211, a Dual SGLT1/SGLT2 Inhibitor, Plus Sitagliptan on Postprandial Active GLP-1 and Glycemic Control in Type 2 Diabetes. *Clin. Ther.* **2013**, *35*, 273-285.

(47) Sands, A. T.; Zambrowicz, B. P.; Rosenstock, J.; Lapuerta, P.; Bode, B. W.; Garg, S. K.; Buse, J. B.; Banks, P.; Heptulla, R.; Rendell, M.; Cefalu, W. T.; Strumph, P. Sotagliflozin, a Dual SGLT1 and SGLT2 Inhibitor, as Adjunct Therapy to Insulin in Type 1 Diabetes. *Diabetes Care* **2015**, *38*, 1181-1188.

(48) Zambrowicz, B. P.; Lapuerta, P.; Strumph, P.; Banks, P.; Wilson, A.; Ogbaa, I.; Sands, A.; Powell, D. LX4211 Therapy Reduces Postprandial Glucose Levels in Patients With Type 2 Diabetes Mellitus and Renal Impairment Despite Low Urinary Glucose Excretion. *Clin. Ther.* **2015**, *37*, 71-82.

(49) Kohan, D. E.; Fioretto, P.; Tang, W.; List, J. F. Long-term Study of Patients with Type 2 Diabetes and Moderate Renal Impairment Shows that Dapagliflozin Reduces Weight and Blood Pressure but Does Not Improve Glycemic Control. *Kidney Int.* **2014**, *85*, 962-971.

(50) Yale, J. F.; Bakris, G.; Cariou, B.; Yue, D.; David-Neto, E.; Xi, L.; Figueroa, K.; Wajs, E.; Usiskin, K.; Meininger, G. Efficacy and Safety of Canagliflozin in Subjects with Type 2 Diabetes and Chronic Kidney Disease. *Diabetes Obes. Metab.* **2013**, *15*, 463-473.

(51) Barnett, A. H.; Mithal, A.; Manassie, J.; Jones, R.; Rattunde, H.; Woerle, H. J.; Broedl, U. D. Efficacy and Safety of Empagliflozin Added to Existing Antidiabetes Treatment in Patients with Type 2 Diabetes and Chronic Kidney Disease: A Randomized, Double-blind, Placebo-controlled Trial. *Lancet Diabetes Endocrinol.* **2014**, *2*, 369-384.

(52) Rawlins, D. B.; Frazier, K. S.; Freiman, J.; Goodwin, N. C.; Harrison, B. A.; Healy, J.; Mabon, R.; Powell, D. R. Discovery and Development of LX4211, a Dual SGLT1 and SGLT2 Inhibitor for the Rreatment of Type 2 Diabetes Mellitus. *Abstracts of Papers, 243rd ACS National Meeting & Exposition*, San Diego, CA, United States, March 25-March 29, 2012, MEDI-19.

(53) Synthetic chemistry on this program ran from 2011-2012.

(54) Kakinuma, H.; Kobashi, Y.; Hashimoto, Y.; Oi, T.; Takahashi, H.; Amada, H.; Iwata, Y. Preparation of C-Phenyl Glycosides as Antidiabetic Human SGLT1 and SGLT2 Inhibitors. PCT Int. Appl. WO 2007136116, 2007.

(55) Kakinuma, H.; Kobashi, Y.; Takahashi, H.; Oi, T.; Hashimoto, Y. Pyrazolyl 5-Thioglucoside Compounds and Antidiabetic Agents Containing the Same. PCT Int. Appl. WO 2007129668, 2007.

(56) Kakinuma, H.; Takahashi, H.; Hashimoto, Y.; Kobashi, Y.; Oi, T. Phenyl 5-Thioglucoside Compounds Having SGLT1 Inhibitory Activities. PCT Int. Appl. WO 2007126117, 2007.

(57) Fushimi, N.; Fujikura, H.; Shiohara, H.; Teranishi, H.; Shimizu, K.; Yonekubo, S.; Ohno, K.; Miyagi, T.; Itoh, F.; Shibazaki, T.; Tomae, M.; Ishikawa0Takemura, Y.; Nakabayashi, T.; Kamada, N.; Ozawa, T.; Kobayashi, S.; Isaji, M. Structure-activity Relationship Studies of 4-Benzyl-1*H*-pyrazol-3-yl β-D-Glucopyranoside Derivatives as Potent and Selective Sodium Glucose Co-transporter 1 (SGLT1) Inhibitors with Therapeutic Activity on Postprandial Hyperglycemia. *Bioorg. Med. Chem.* **2012**, *20*, 6598-6612.

(58) Fushimi, N.; Teranishi, H.; Shimizu, K.; Yonekubo, S.; Ohno, K.; Miyagi, T.; Itoh, F.; Shibazaki, T.; Tomae, M.; Ishikawa-Takemura, Y.; Nakabayashi, T.; Kamada, N.; Yamauchi, Y.; Kobayashi, S.; Isaji, M. Design, Synthesis, and Structure-activity Relationships of a Series of 4-Benzyl-5-isopropyl-1*H*-pyrazol-3-yl β-D-Glycopyranosides Substituted with Novel Hydrophlic Groups as Highly Potent Inhibitors of Sodium Glucose Co-transporter 1 (SGLT1). *Bioorg. Med. Chem.* **2013**, *21*, 748-765.

(59) Shibazaki, T.; Tomae, M.; Ishikawa-Takemura, Y.; Fushimi, N.; Itoh, F.; Yamada, M.; Isaji, M. KGA-2727, a Novel Selective Inhibitor of a High-Affinity Sodium Glucose Cotransporter (SGLT1), Exhibits Antidiabetic Efficacy in Rodent Models. *J. Pharmacol. Exp. Ther.* **2012**, *342*, 288-296.

(60) Intestinal and liver metabolic stability were monitored. The compounds presented here had no liabilities in these experiments and the data are thus not presented in this manuscript.

(61) Beesley, R. M.; Ingold, C. K.; Thorpe, J. F. CXIX. – The Formation and Stability of Spiro-compounds. Part I. *Spiro*-Compounds from *Cyclo*hexane. *J. Chem. Soc., Trans.* **1915**, 1080-1106.

(62) Jung, M. E.; Piizzi, G. *gem*-Disubstitutent Effect: Theoretical Basis and Synthetic Applications. *Chem. Rev.* **2005**, *105*, 1735-1766.

(63) Carson, K. G.; Goodwin, N. C.; Harrison, B. A.; Rawlins, D. B.; Strobel, E. S.; Zambrowicz, B. Preparation of Glycosides as Antidiabetic Inhibitors of SGLT1. PCT Int. Appl. WO2014081660, 2014.

(64) Powell, D. R.; DaCosta, C. M.; Smith, M.; Doree, D.; Harris, A.; Buhring, L.; Heydorn, W.; Nouraldeen, A.; Xiong, W.; Yalamanchili, P.; Mseeh, F.; Wilson, A.; Shadoan, M.; Zambrowicz, B.; Ding, Z. Effect of LX4211 on Glucose Homeostasis and Body Composition in Preclinical Model. *J. Pharmacol. Exp. Ther.* **2014**, *350*, 232-242.

(65) Goodwin, N. C.; Harrison, B. A.; Iimura, S.; Mabon, R.; Song, Q.; Wu, W.; Yan, J.; Zhang, H.; Zhao, M. M. Preparation of Glycosyl Sulfoxides as Potential Antidiabetic Sodium Glucose Co-transporter 2 Inhibitors. PCT Int. Appl. WO 2009014970, 2009.

(66) Littke, A. F.; Fu, G. C. A Versatile Catalyst for Heck Reactions of Aryl Bromides and Aryl Chlorides under Mild Conditions. *J. Am. Chem. Soc.* **2001**, *123*, 6989-7000.

Table of Contents Graphic

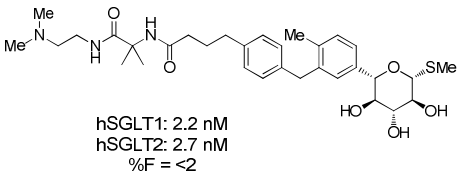

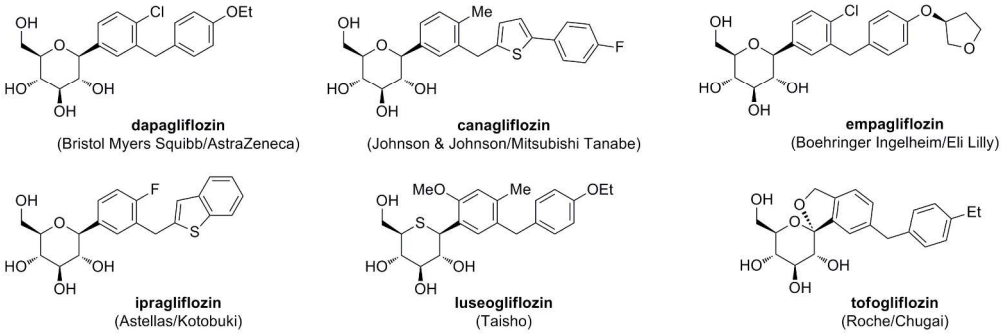

Figure 1. Marketed SGLT2 inhibitors (2016).
Dapagliflozin20-22 and canagli
229x76mm (300 x 300 DPI)

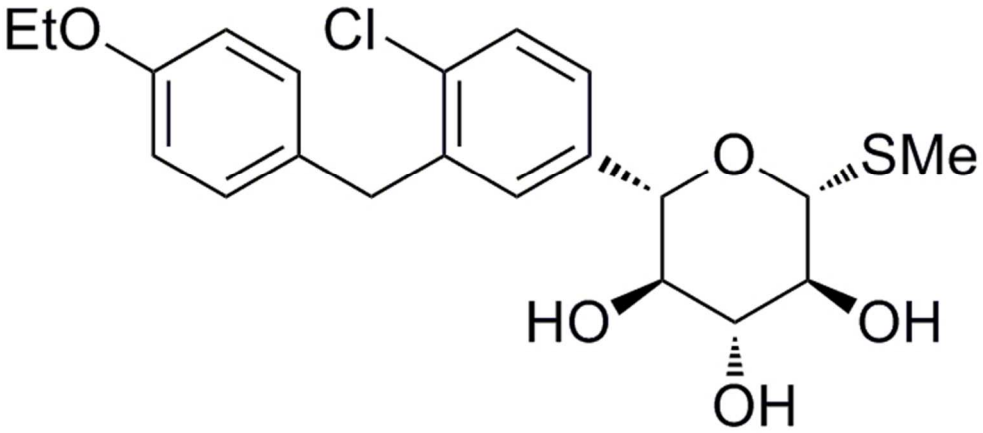

Figure 2. Sotagliflozin (1), a dual SGLT1/2 inhibitor in clinical trials for type 1 and type 2 diabetes. The added benefit of inhibitin
60x27mm (300 x 300 DPI)

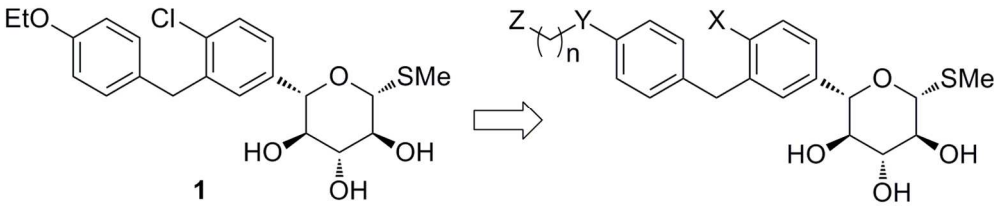

Figure 3. Synthetic strategy to design a compound that is restricted to the lumen starting with the xyloside core of 1.
As highlighted in Figure 3, ch
132x27mm (300 x 300 DPI)

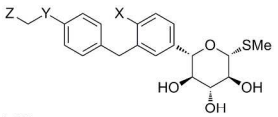

Cmpd	X	Y	Z	IC_{50} (nM) hSGLT1	IC_{50} (nM) hSGLT2	%F[a]
1	Cl	O	Me	36.2	1.8	98
2	Cl	O	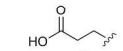	250	4.3	
3	Me	O	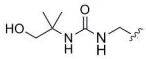	48.2	3.7	
4	Me	O	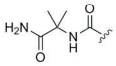	25.3	5.2	
5	Me	O		15.4	14.5	18
6	Cl	O	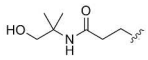	2.4	0.9	17
7	Me	O	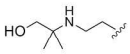	3.3	2.5	1.1
8	Me	O	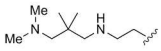	2.0	1.6	BLQ
9	Me	CH_2	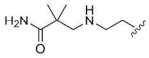	2.3	3.6	0.5
10	Me	O	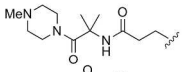	2.9	3.7	0.4
11	Me	CH_2	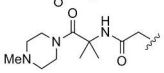	1.8	1.9	BLQ

[a] measured at 10mpk, PO. BLQ = not available due to insufficient compound level in plasma

Table 1. Representative SAR of non-absorbable dual SGLT1/2 inhibitors.
A brief summary of substitutio
241x124mm (300 x 300 DPI)

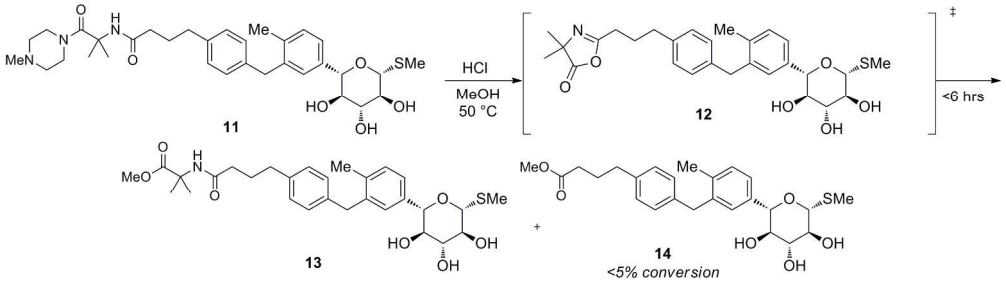

Figure 4. Synthetic instability of piperazine amide 11.
As shown in Figure 4,
229x65mm (300 x 300 DPI)

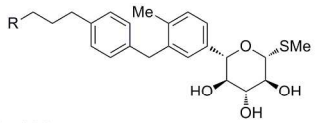

Cmpd	R	IC_{50} (nM) hSGLT1	IC_{50} (nM) hSGLT2	stable to hydrolysis?[a]
11	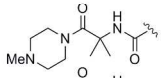	1.8	1.9	no[b]
15	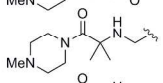	14.8	3.1	yes[c]
16	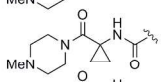	1.1	2.5	no
17	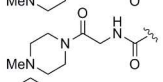	8.4	2.5	no
18	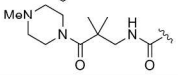	6.8	3.4	no
19	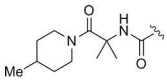	1.6	2.5	no
20	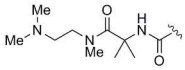	1.7	1.3	yes
21	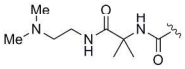	2.2	2.7	yes
22	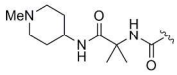	2.7	3.7	yes

[a] 50/50 1N aq. HCl/MeOH, 50 °C, 72 hrs. [b] >5% degradation. [c] <5% degradation

Table 2. Stability of replacements to the hydrolytically-labile bis-amide motif of 11
All compounds shown in Table 2
227x123mm (300 x 300 DPI)

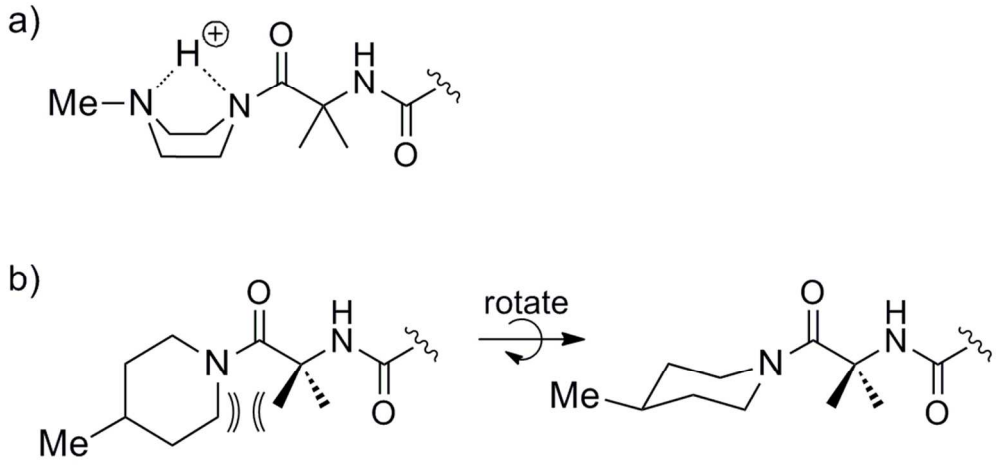

Figure 5. Destabilizing conformations of cyclic amides. (A) Acid-promoted conformational change of piperidinylamide engages nitrogen lone pair and destabilizes the carbonyl. (B) Unfavorable steric interaction of piperidinyl-amide with gem-dimethyl group favors a conformation that removes the nitrogen lone pair from conjugation with the carbonyl.
The last approach examined the
95x44mm (300 x 300 DPI)

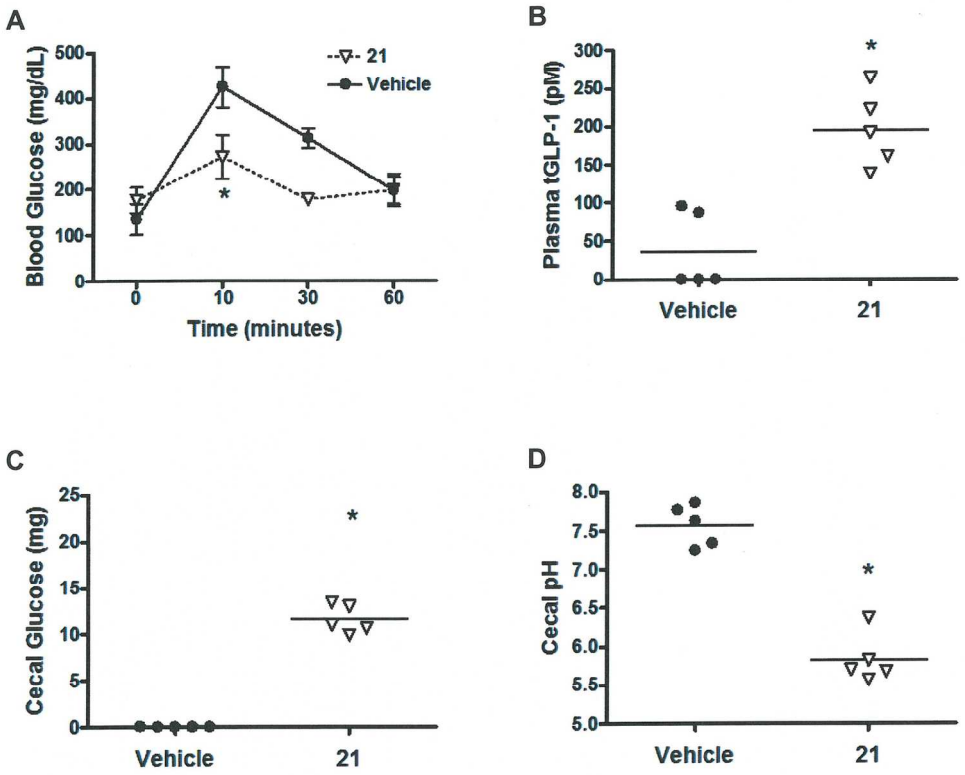

Figure 6. Compound 21 delays intestinal glucose absorption and increases postprandial tGLP-1 levels in mice. Individual healthy mice received either vehicle (□) or 21 at a dose of 1.5 mg/kg (21, ρ) by oral gavage for 4 consecutive days and then, 22 hours later after a 16 hour fast, received a glucose-containing meal challenge by oral gavage. A) Blood samples were collected through retro-orbital bleeding at 0, 10 30 and 60 minutes after meal challenge, and glucose AUC was calculated for each glucose excursion. At 60 minutes after the meal challenge (23 hours after the dose of compound or vehicle), mice were necropsied; blood samples collected at that time were used to measure B) plasma tGLP-1 levels, and cecal contents collected at that time were analyzed for C) total cecal glucose and D) cecal pH. * Different from vehicle, P < 0.001.

The results from the oral gluc

148x119mm (300 x 300 DPI)

	dose	*N*	half life	$AUC_{0-\infty}$	V_{ss}	CL
I.V.	*mg/kg*		*hr*	*nM*hr*	*L/kg*	*mL/min/kg*
compound **21**	1	4	0.4 ± 0.0	693 ± 107	1.3 ± 0.3	40.3 ± 6.6
compound **1**	1	4	1.39 ± 0.45	1940 ± 331	2.07 ± 0.14	20.6 ± 3.0

CL, clearance; *N*, number of animals, V_{ss}, volume at steady state

	dose	*N*	half life	C_{max}	$AUC_{0-\infty}$	%F
P.O.	*mg/kg*		*hr*	*nM*	*nM*hr*	
compound **21**	10	4	N/A	43 ± 11	N/A	N/A
compound **1**	10	4	6.52 ± 0.82	4973 ± 408	19709 ± 1580	98 ± 8

N/A, not available due to lack of terminal phase or insufficient compound levels in plasma

Figure 7. Pharmacokinetic data comparing compounds 21 and 1 at 1mg/kg IV and 10 mg/kg (PO). The results of mouse pharmacok
198x67mm (300 x 300 DPI)

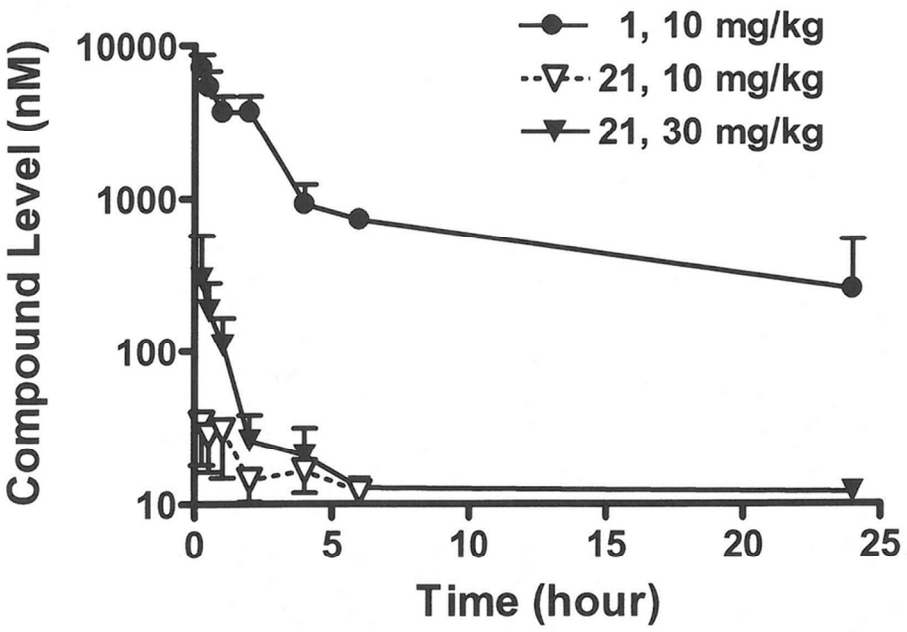

Figure 8. Plasma concentration-time course comparing compounds 21 and 1 at 10 and 30 mg/kg after oral administration.
Figure 8 shows the striking di
85x63mm (300 x 300 DPI)

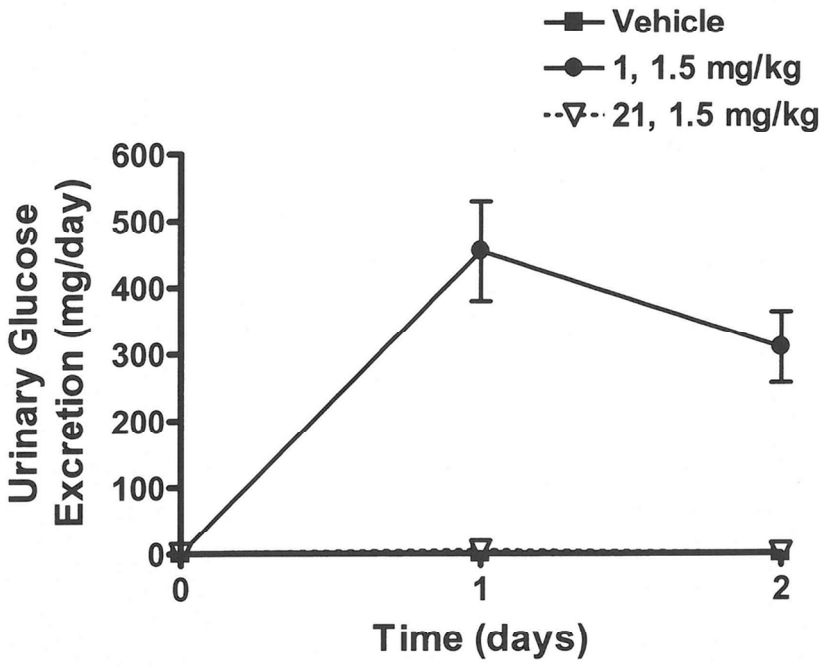

Figure 9. Urinary glucose excretion comparing a single 1.5 mg/kg dose of 21 and 1 before (day 0) and after (days 1 and 2) administration by oral gavage.
As shown in Figure 9, 21 had l
105x84mm (300 x 300 DPI)

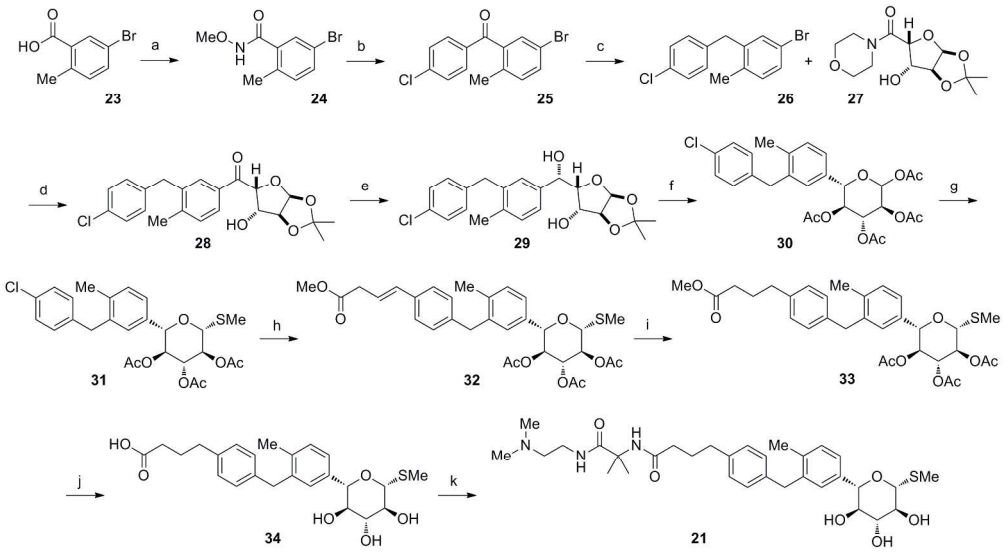

Scheme 1. Synthesis of 21. Reagents and conditions: (a) (COCl)2, DMF (cat.), CH2Cl2; MeNH(OMe)•HCl, Et3N, CH2Cl2; 99% yield (b) (4-chlorophenyl)magnesium chloride, THF, 0 °C; 99% yield (c) Et3SiH, BF3•OEt2, CH3CN, 60 °C; 62% yield (d) n-BuLi, THF, −78 °C, then 27/t-BuMgCl, THF, 0 °C to 23 °C; 70% yield (e) NaBH4, CeCl3•7H2O, MeOH; 99% yield (f) HOAc/H2O, 100 °C; Ac2O, Et3N, CH3CN; 92% yield (g) TMSOTf, thiourea, dioxane, 80 °C; MeI then DIPEA, 23 °C; 60% yield (h) methyl but-3-enoate, Pd2dba3, [t-Bu3PH]BF4, Cy2NMe, NMP, 160 °C, microwave irradiation; 60% yield (i) H2, Pd/C; 94% yield (j) LiOH, MeOH/H2O; 99% yield (k) 2-amino-N-(2-(dimethylamino)ethyl)-2-methylpropanamide hydrochloride, HATu, DIPEA, DMF; 40% yield after prep HPLC.
medicinal chemistry synthesis
237x130mm (300 x 300 DPI)

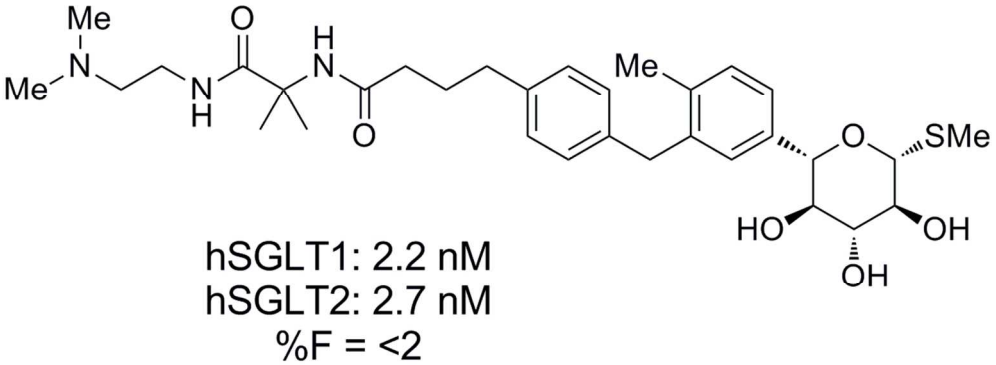

108x40mm (300 x 300 DPI)